Earth-Science Reviews 185 (2018) 665–683

Contents lists available at ScienceDirect

Earth-Science Reviews

journal homepage: www.elsevier.com/locate/earscirev

Geochronology of shear zones – A review

Sebastián Oriolo[a,*], Klaus Wemmer[b], Pedro Oyhantçabal[c], Haakon Fossen[d], Bernhard Schulz[e], Siegfried Siegesmund[b]

[a] Instituto de Geociencias Básicas, Aplicadas y Ambientales de Buenos Aires (IGEBA), CONICET-Universidad de Buenos Aires, Intendente Güiraldes 2160, Buenos Aires C1428EHA, Argentina
[b] Geoscience Center, Georg-August-Universität Göttingen, Goldschmidtstraße 3, Göttingen 37077, Germany
[c] Departamento de Geodinámica Interna, Facultad de Ciencias, Universidad de la República, Iguá 4225, Montevideo 11400, Uruguay
[d] Museum of Natural History, Department of Earth Science, University of Bergen, Box 7803, Bergen 5020, Norway
[e] TU Bergakademie Freiberg, Institute of Mineralogy, Brennhausgasse 14, Freiberg D-09596, Germany

ARTICLE INFO

Keywords:
Thermochronology
Closure temperature
Isotopic diffusion
Mylonites
Strain localization
Deformation mechanisms

ABSTRACT

Shear zones play a major role in the deformation of the crust at a variety of scales, as expressions of strain localization during orogeny and rifting, and also as reactivated structures. They influence the geometry and evolution of orogenic belts and rifts, crustal rheology, magma ascent and emplacement, and fluid flow. Consequently, assessing the timing of shear zone activity is crucial to reconstruct the tectonometamorphic evolution of the lithosphere. The interpretation of thermochronologic data from shear zones is, however, not straightforward. In the first place, closure temperatures depend on a number of factors (grain size, cooling rate, mineral composition and pressure, among others). On the other hand, deformation-related processes such as dynamic recrystallization, neocrystallization and fluid circulation seem to be crucial for isotopic systems and, thus, the obtained ages cannot be solely interpreted as a function of temperature in sheared rocks. For this reason, geochronologic data from shear zones might not only record cooling below closure temperature conditions but may also be affected by neo- or recrystallization, fluid-assisted deformation and inheritance of the protolith age(s). In order to robustly reconstruct P-T-ε-t paths of long-term crustal-scale shear zones, structural, microstructural and petrologic data from mylonites need to be integrated with ages from different thermochronometric systems. In addition, geochronologic data from associated intrusions and adjacent blocks can provide further irreplaceable constraints on the timing of deformation and its regional implications. One of the most challenging aspects that future lines of investigation should analyze is the quantitative evaluation of so far poorly explored aspects of isotopic diffusion, particularly the coupling with deformation processes, based on natural, theoretical and experimental data. Future works should also investigate the role of strain partitioning and localization processes in order to constrain the timing of deformation in different parts of a shear zone or in different branches of anastomosing shear zone networks.

1. Introduction

Shear zones are strain localization features that occur at all scales in the lithosphere and significantly control magma emplacement, fluid circulation, rift development and orogenic evolution, thus being one of the main controls on lithosphere rheology (Ramsay, 1980; Sibson, 1990; Brown and Solar, 1998; Micklethwaite et al., 2010; Vauchez et al., 2012; Montési, 2013; Clerc et al., 2015; Smeraglia et al., 2016; Fossen and Cavalcante, 2017; Précigout et al., 2017). Assessing the timing of shear zone activity is, therefore, critical to understand crustal deformation behavior in different tectonic settings. However, most shear zones have a complex evolutionary history under variable P-T conditions that frequently involve strain partitioning and localization processes, or even non-steady deformation (e.g., van der Pluijm et al., 1994; Fossen and Tikoff, 1997; Carreras et al., 2010; Oriolo et al., 2016a, 2016b). The complex nature and evolution of natural shear zones largely prevents straightforward interpretation of geochronologic data from such zones, and only integrated structural analysis and detailed geochronology can help to unravel shear zone evolution through time.

The timing of shearing is generally constrained by thermochronology, i.e., by obtaining ages from different isotopic systems that allow the reconstruction of a thermal history (e.g., Braun et al., 2006). Since all isotopic systems are somehow affected by thermal effects, all

* Corresponding author.
E-mail addresses: soriolo@gl.fcen.uba.ar, seba.oriolo@gmail.com (S. Oriolo).

https://doi.org/10.1016/j.earscirev.2018.07.007
Received 19 February 2018; Received in revised form 16 July 2018; Accepted 16 July 2018
Available online 18 July 2018
0012-8252/

isotopic dating can be regarded as thermochronology and, consequently, it is difficult to establish a clear distinction between geo- and thermochronology (Harrison and Zeitler, 2005; Reiners et al., 2005). However, geochronology and thermochronology exhibit some differences, particularly in terms of their scopes. For instance, the crystallization age of minerals is fundamental in geochronology, aiming to provide an absolute temporal constraint on a magmatic or stratigraphic age (Reiners et al., 2005). Such questions are rather irrelevant for thermochronology which, instead, focuses on duration and rates of processes (Reiners et al., 2005). In the case of shear zones, isotopic data are mostly interpreted in the light of thermochronology, though other factors may play a major role in isotopic diffusion as well (see below). There is, therefore, a fuzzy boundary between geochronology and thermochronology, which is intrinsically related to processes occurring in shear zones.

In shear zones, thermochronologic data can be obtained directly from mylonitic rocks or from blocks adjacent to the shear zone, whereas crystallization ages of associated magmatic rocks may provide further constraints (van der Pluijm et al., 1994; Oriolo et al., 2016a). Thermochronologic methods consider isotopic diffusion to be primarily governed by temperature and, hence, isotopic systems are interpreted in terms of their characteristic closure temperatures (Dodson, 1973). When combined with microstructural and/or thermobarometric data, cooling and exhumation rates can be derived and, therefore, thermochronology allows for reconstruction of P-T-ε-t (pressure-temperature-strain-time) paths of sheared regions. Nevertheless, isotopic diffusion might not be solely controlled by temperature, but may also be influenced by solid-state processes such as recrystallization, fluid circulation and metamorphic reactions (Dunlap, 1997; Villa, 1998; Mulch and Cosca, 2004; Harley et al., 2007; Tagami, 2012; Harlov, 2015; Oriolo et al., 2016a), all of which are ubiquitous in shear zones. In addition to complex structural histories (e.g., Carreras et al., 2013; Druguet et al., 2018), ambiguities concerning diffusion thus pose a challenge for the interpretation of geochronologic data from shear zones.

A recent debate on the evolution of the Cap de Creus shear zone network (eastern Pyrenees) has highlighted controversies about the meaning of shear zone geochronologic data (Vissers et al., 2016; Druguet et al., 2018), despite being one of the most well-known shear zone systems in the world (Carreras and Druguet, 1994; Carreras, 2001; Druguet, 2001; Carreras et al., 2005, 2013; Druguet et al., 1997, 2013). $^{40}Ar/^{39}Ar$ muscovite data from mylonites were presented by Vissers et al. (2016), who interpreted these ages as the result of shear zone activity during Jurassic extension. In contrast, Druguet et al. (2018) emphasized structural evidence pointing to a Late Paleozoic deformation age related to the Variscan orogeny, arguing that muscovite ages result from partial resetting of the $^{40}Ar/^{39}Ar$ system (i.e., partial Ar loss due to thermal overprinting) during Meso-Cenozoic thermal events and do not constrain the timing of shearing. Druguet et al. (2018) challenged the interpretation of Vissers et al. (2016), emphasizing that diffusion parameters have to be calculated for a robust evaluation of their $^{40}Ar/^{39}Ar$ data.

In recent years, several contributions have summarized and revised structural, microstructural, geometric and rheologic aspects of shear zones (Carreras et al., 2005, 2010; Xypolias, 2010; Platt and Behr, 2011a, 2011b; Law, 2014; Cao and Neubauer, 2016; Fossen and Cavalcante, 2017; Passchier and Platt, 2017). On the other hand, robust models of shear zone evolution based on combined structural, microstructural, geochronologic and petrologic data are still scarce, as recently emphasized by Fossen and Cavalcante (2017). For this reason, this contribution aims to provide guidelines and some “notes of caution” for the evaluation and interpretation of geochronologic data in shear zones, based on a general background on diffusion-related processes, closure temperature, and structural and microstructural aspects. Details on particular geochronologic methods and systems are outside of the scope of the manuscript, for which the reader is referred to more specific contributions. Although several aspects of shear zone dating presented herein are also valid for other metamorphic and even igneous rocks, the focus is placed on ductile shear zones, regarded as high-strain tabular zones following the classical definition of Ramsay, 1980 see also (Fossen and Cavalcante, 2017). In this sense, geochronology of mylonites recording ductile deformation (> 300 °C) is emphasized, though some considerations regarding shear zone rocks related to brittle-ductile and brittle deformation (e.g., fault gouge, pseudotachylites) are presented as well (e.g., Sibson, 1977; Fossen and Cavalcante, 2017).

2. Introduction to geochronology and analytical methods

The basic principle of isotopic geology is the radioactive decay, i.e., the radioactive disintegration of a parent isotope to a daughter isotope. Radioactive decay is independent of external physical and chemical effects and occurs at a rate related to the amount of parent nuclide and a decay constant λ that represents the likelihood that a radioactive disintegration takes place in a certain unit of time (e.g., Vermeesch, 2015). In this contribution, two main groups of isotopic systems are considered, due to their massive application in shear zone-related and other metamorphic rocks: those related to the U-Th-Pb system, mostly used for high-temperature thermochronology (> 600 °C), and those associated with the K-Ar and Rb-Sr systems, applied to medium to low-temperature conditions (Section 3, Table 1).

The U-Th-Pb system is one of the most used isotopic systems in geochronology, due to the abundance of high-U minerals (e.g., zircon, monazite, titanite, rutile, apatite), which are significantly resistant to chemical and physical weathering (Schoene, 2014, and references therein). This isotopic system is based on the U-Th-Pb decay series, which comprise the decay of ^{238}U, ^{235}U and ^{232}Th to ^{206}Pb, ^{207}Pb and ^{208}Pb, respectively, with $\lambda_{238} = 1.551359 \times 10^{-10}\,y^{-1}$, $\lambda_{235} = 9.845841 \times 10^{-10}\,y^{-1}$ and $\lambda_{232} = 4.933431 \times 10^{-11}\,y^{-1}$ (Vermeesch, 2015). In general, three main analytical techniques have been applied to U-Th-Pb dating: ID-TIMS (isotope-dilution thermal ionization mass spectrometry), LA-ICP-MS (laser ablation inductively-coupled plasma mass spectrometry) and SIMS (secondary ion mass spectrometry), the latter of which also includes the SHRIMP (sensitive high-resolution ion microprobe) method (e.g., Schaltegger et al., 2015, and references therein). ID-TIMS is a high-precision, whole-grain method, whereas SIMS and LA-ICP-MS present a higher spatial resolution and are thus more adequate to date crystals recording a polyphase evolution (e.g., Schaltegger et al., 2015). In turn, SHRIMP requires a smaller spot for analysis than LA-ICP-MS, thus being more adequate for complex crystal zonation patterns, such as metamorphic zircons (Kröner et al., 2014). In all cases, these methods require a mechanical separation of the mineral fraction to be dated. In contrast, *in situ* methods such as the electron microprobe (EMP) Th-U-Pb dating of

Table 1
Estimated closure temperature (T_c) for different isotopic systems, commonly used (or potentially applicable) to date shear zones.

	T_c (°C)	References
U, Th, Pb zircon	> 900	Lee et al. (1997), Cherniak and Watson (2000)
Th, Pb monazite	> 900	Cherniak et al. (2004), Cherniak and Pyle (2008)
Pb titanite	650 ± 50	Cherniak (1993), Dahl (1997), Frost et al. (2000)
Pb rutile	600 ± 100	Cherniak (2000), Vry and Baker (2006), Kooijman et al. (2010)
Sm, Nd garnet	600 ± 30	Mezger et al. (1992a)
Sr muscovite	500 ± 50	Jäger et al. (1967), Jäger (1977)
Ar hornblende	530 ± 40	Harrison (1981)
Pb apatite	450 ± 100	Chamberlain and Bowring (2000), Schoene and Bowring (2007), Chew and Spikings (2015)
Ar muscovite	350–425	Purdy and Jäger (1976), Harrison et al. (2009)
Sr biotite	350 ± 50	Jäger (1977), Verschure et al. (1980)
Ar biotite	310 ± 40	Harrison et al. (1985), Grove and Harrison (1996)

monazite (Suzuki et al., 1991; Montel et al., 1996; Spear et al., 2009) allow obtaining ages from polished thin sections, permitting to interpret the resulting age in a microstructural context (see also Section 6.1).

On the other hand, the K-Ar system has been widely used to date shear zones, since it can be applied within medium to low temperature ranges, common in natural shear zones (Table 1, Section 3). This system is based on the decay of ^{40}K to ^{40}Ar via electron capture followed by γ decay or directly by electron capture, with a combined $\lambda_{40} = 0.581 \times 10^{-10}\ y^{-1}$ (Steiger and Jäger, 1977). In the K-Ar method, K is measured by conventional chemical methods (e.g., flame photometry, atomic absorption spectroscopy, isotope dilution), whereas Ar isotopes are determined on a separate aliquot (e.g., Kelley, 2002, and references therein). In contrast, the $^{40}Ar/^{39}Ar$ technique allows to measure both in the same aliquot, since K is measured by irradiating the sample in a nuclear reactor, creating ^{39}Ar from ^{39}K by neutron bombardment (e.g., McDougall and Harrison, 1999; Kelley, 2002). In particular, the stepwise heating approach for $^{40}Ar/^{39}Ar$ permits to verify premises of closed system, based on the presence of the so called "plateau age" pattern (e.g., McDougall and Harrison, 1999). Similarly to *in situ* monazite dating, *in situ* $^{40}Ar/^{39}Ar$ dating also allows interpreting ages in their microstructural setting (e.g., Di Vincenzo et al., 2001; Mulch et al., 2002; Mulch and Cosca, 2004). $^{40}Ar/^{39}Ar$ seems to be, however, problematic in the case of fine-grained K-bearing minerals (illite, white mica), essentially due to ^{39}Ar recoil arising from neutron flow during irradiation, for which K-Ar seems to be more adequate (Clauer et al., 2012; Clauer, 2013). In this sense, the combination of K-Ar dating of fine mineral fractions with X-ray diffraction (XRD) data allows the quantification of the crystallinity index (Kübler Index), which is useful in order to assess temperature conditions and to discriminate between neoformed and inherited crystals (e.g., Kübler, 1964; Frey, 1987; Kisch, 1987; Löbens et al., 2011; Wemmer et al., 2011; Doublier et al., 2015; Viola et al., 2016; Bense et al., 2017).

Finally, the Rb-Sr dating is based on the β^- decay of ^{87}Rb to ^{87}Sr with a $\lambda_{87} = 1.41 \times 10^{-11}\ y^{-1}$ (Steiger and Jäger, 1977), though some modifications to the decay constant have been suggested during the last decades (Villa et al., 2015, and references therein). In terms of analytical approaches, Rb-Sr isotopes have been classically separated using standard cation exchange procedures and subsequently measured by TIMS, though some attempts by LA-ICP-MS have been presented in the last years (e.g., García-Ruiz et al., 2008; Hogmalm et al., 2017).

3. Isotopic closure, the Alpha and the Omega

3.1. Closure temperature

The first requirement for the interpretation of isotopic data is the existence of a "closed isotopic system", which implies that the host mineral does not exchange isotopes with its surroundings (e.g., Villa, 1998), since diffusion rates are negligible. In thermochronology, isotopic closure can be understood by means of the closure temperature T_c, which is defined as "the temperature of the system at the time represented by its apparent age" (Dodson, 1973). Once a rock starts cooling and achieves a certain temperature (i.e., open-system temperature), the daughter isotope will start to be retained (Braun et al., 2006). After further cooling, negligible diffusion rates allow retention of the daughter isotope and a closed-system behavior is achieved. The upper temperature limit of this closed-system behavior is the blocking temperature, whereas T_c lies between the open-system and the blocking temperature, within the partial retention zone (Braun et al., 2006). The relationship between thermally activated diffusion D, which is restricted to volume diffusion, and temperature T arises from the Arrhenius equation (Eq. (1); Dodson, 1973; Harrison et al., 2009), where D_0 is the frequency factor, E_a the activation energy and R the gas constant.

$$D = D_0 e^{-E_a/RT} \tag{1}$$

According to Dodson (1973), the T_c of a certain geochronologic system can thus be calculated as:

$$T_c = \frac{E_a}{R \ln\left(\frac{A\tau D_0}{a_s^2}\right)} \tag{2}$$

where A is a constant depending on the geometry and decay constant of the parent isotope, τ the time constant with which D diminishes, and a_s is the characteristic diffusion size (Dodson, 1973). Though Eq. (2) is only valid if T^{-1} increases linearly with time, a good approximation is obtained by relating τ to the slope of the cooling curve at T_c (Dodson, 1973).

Table 1 presents a summary of several thermochronometers and their closure temperatures which are widely applied to reconstruct thermal histories of metamorphic rocks. The first limitation is that E_a and D_0 are experimentally determined and, depending of the applied values for the T_c calculation, the obtained temperatures may vary (e.g., see compilations of Pb and Ar diffusion parameters by Dahl, 1997, and Braun et al., 2006, respectively). Additionally, A takes different values for a sphere, cylinder or plane sheet geometry (Dodson, 1973). For the K-Ar system in muscovite, Harrison et al. (2009) highlighted differences in diffusion parameters arising from the assumption of a plane sheet (Robbins, 1972) or an infinite cylinder geometry (Hames and Bowring, 1994). Differences in A are related to the fact that diffusion depends on the crystallographic structure and is thus strongly anisotropic, i.e., different crystallographic directions exhibit different D values (Hames and Bowring, 1994; Cherniak, 1995; Ganguly et al., 2007; Reich et al., 2007).

Besides values assumed for constants A, E_a and D_0, Eq. (1) shows that closure temperatures depend on the grain size a_s. For instance, many experimental studies consider a_s to be equivalent to the physical grain half width of prismatic minerals (e.g., Farley, 2000) On the other hand, τ can be expressed as a function of cooling rate $\dot{T}$ (e.g., Dodson, 1973; Braun et al., 2006), as follows:

$$\tau = \frac{-RT^2}{E_a \dot{T}} \tag{3}$$

Eq. (1) can thus be rewritten as shown in Eq. (4), which can be solved by an iterative determination considering that T_c appears on both sides (Dodson, 1973).

$$T_c = \frac{E_a}{R \ln\left(\frac{-ART_c^2 D_0}{a_s^2 E_a \dot{T}}\right)} \tag{4}$$

According to Eq. (4), it is evident that T_c also varies as a function of the cooling rate $\dot{T}$. In order to evaluate the influence of the different parameters, variations of closure temperatures for the Ar diffusion in different minerals that are commonly applied in shear zone studies are illustrated in Fig. 1, considering a grain size range of 100-500 μm and cooling rates within the range of natural shear zones (ca. 5-100 °C/my; Grégoire et al., 2009; Webb et al., 2010; Bonamici et al., 2014; Oriolo et al., 2016a). In the particular case of feldspars, vacuum experiments on Ar diffusion reveal subparallel arrays in the $\log(D/a_s^2)$ vs (10000/T) diagram and, therefore, Ar diffusivity can be characterized in subdomains with different a_s (e.g., Lovera et al., 1989).

3.2. Further controls on isotopic closure

Besides closure temperature and its controlling parameters, other factors might also influence isotopic closure. Some of the most important are pressure, mineral composition, neo-/recrystallization and fluids (Dunlap, 1997; Villa, 1998; Mulch and Cosca, 2004; Tagami, 2012; Harlov, 2015; Oriolo et al., 2016a). Since the latter two are of particular importance in shear zones, they are treated separately (see Section 3.3).

The diffusion model of Dodson was formulated at isobaric

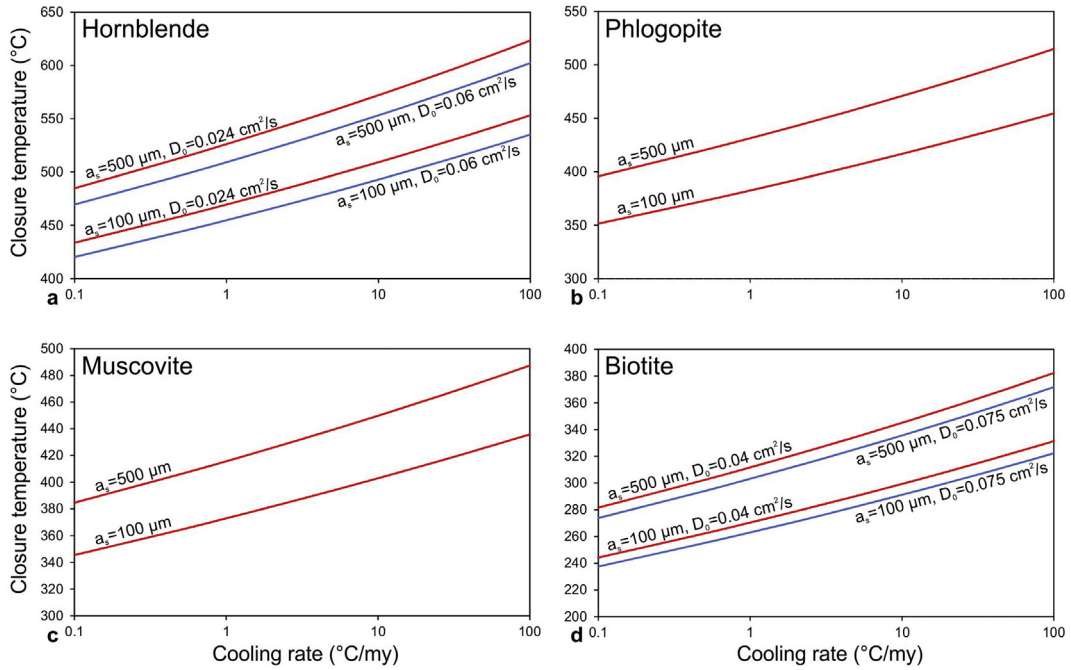

Fig. 1. Variation of closure temperature as a function of cooling rate and effective diffusion radius (a_s) for different minerals. In the case of hornblende and biotite, variations arising from different input parameters (frequency factor D_0) are also shown. Variation of closure temperature with composition are illustrated by Fe-Mg micas (i.e., phlogopite and biotite) based on X_{annite}. Closure temperatures were calculated using Closure 1.2 (Brandon et al., 1998; Brandon, 2007). a) Hornblende (experimental data: E_a = 268 kJ·mol^{-1}, D_0 = 0.060 cm^2·s^{-1}, Harrison, 1981; experimental and geological data: E_a = 268 kJ·mol^{-1}, D_0 = 0.024 cm^2·s^{-1}, Harrison, 1981). b) Phlogopite, X_{annite} = 0.04 (E_a = 242 kJ·mol^{-1}, D_0 = 0.075 cm^2·s^{-1}, Giletti, 1974). c) Muscovite (E_a = 267.8 kJ·mol^{-1}, D_0 = 20 cm^2·s^{-1}, Harrison et al., 2009). d) Biotite, X_{annite} = 0.55 (E_a = 197 kJ·mol^{-1}, D_0 = 0.075 cm^2·s^{-1}, Harrison et al., 1985; Grove and Harrison, 1996) and X_{annite} = 0.71 (E_a = 197 kJ·mol^{-1}, D_0 = 0.04 cm^2·s^{-1}, Grove and Harrison, 1996).

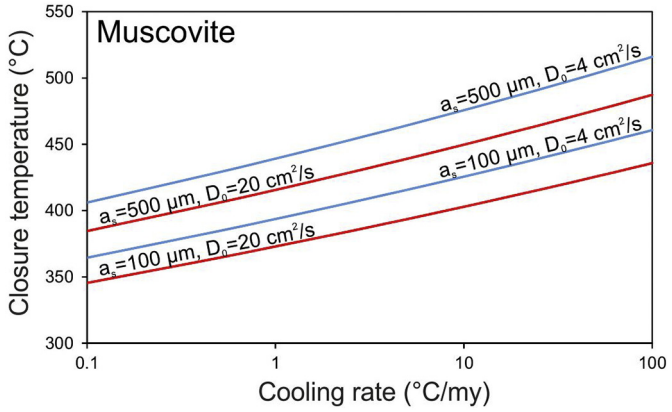

Fig. 2. Variation of closure temperature as a function of cooling rate and effective diffusion radius (a_s) for muscovite, considering E_a = 267.8 kJ·mol^{-1} and different frequency factor values for pressures of 5 (D_0 = 20 cm^2·s^{-1}) and 10 kbar (D_0 = 4 cm^2·s^{-1}) (modified after Harrison et al., 2009). Closure temperatures were calculated using Closure 1.2 (Brandon et al., 1998; Brandon, 2007).

conditions, and the influence of pressure on closure temperatures has been poorly evaluated. However, Arrhenius parameters used for closure temperature calculations may vary with pressure (Fig. 2; Harrison et al., 1985, 2009; Villa et al., 2014). For instance, Harrison et al. (2009) indicated D_0 = 4 cm^2·s^{-1} for Ar closure in muscovite at 10 kbar, whereas a value of D_0 = 20 cm^2·s^{-1} was calculated for the same system at 5 kbar, considering an activation volume of 14 cm^3·mol^{-1}. Predicted closure temperatures show differences of ca. 20-30 °C (Fig. 2; Harrison et al., 2009). In the same way, Lister and Baldwin (1996) indicated higher closure temperatures for white mica in high-pressure than in low-pressure rocks. An interesting attempt to quantitatively evaluate pressure effects in diffusion process was recently presented by Liang (2017), who modified Dodson's (1973) formulation to obtain corrected pressure-dependent equations for T_c calculations.

In addition to pressure, mineral composition might also affect Arrhenius parameters used for T_c calculations. This is particularly relevant for biotite, which shows significant differences in D_0 and E_a values for Ar closure depending on the Fe/Mg ratio, which, in turn, results in variations in Ar retentivity and significantly different closure temperatures (Fig. 1; Harrison et al., 1985; Grove and Harrison, 1996; Braun et al., 2006). Closure temperature of the Rb-Sr system in biotite is also affected by mineral compositions, since it is influenced by Rb and Sr contents and their partition coefficients (Jenkin et al., 2001). Additionally, modal composition of the rock affects the closure temperature of Sr diffusion in both muscovite and biotite due to cation exchange processes (Jenkin, 1997; Jenkin et al., 2001).

3.3. Deformation-related processes

Deformation-related processes such as recrystallization, neocrystallization and fluid circulation are well-documented solid-state phenomena playing a major role in isotopic exchange (Villa, 1998). All these variables are intimately related since, on one hand, fluids can be released during breakdown of hydrous minerals, thus favoring strain localization and deformation, whereas the latter promotes changes in porosity and permeability that, on the other hand, affect fluid flow (e.g., Kolb, 2008; Mittempergher et al., 2014; Fossen and Cavalcante, 2017; Violay et al., 2017). When present, fluid-assisted (re)crystallization is a more efficient mechanism for isotopic exchange than thermally activated diffusion and, hence, it will be the main controlling factor (Villa, 1998). In addition, sub-microscopic and lattice defects related to deformational microstructures may also play a major role in isotopic diffusion, as shown for Ar in both naturally and experimentally deformed micas (Mulch et al., 2002; Cosca et al., 2011). This means

that, in many cases, isotopic ages cannot be directly interpreted as "cooling ages", thus complicating the reconstruction of true T-t cooling paths. Instead, ages might represent the timing of mineral (re)crystallization and/or hydrothermal fluid circulation, as these deformation-related processes lead to resetting of the isotopic system mostly at or below T_c temperature conditions.

Combined $^{40}Ar/^{39}Ar$ diffusion experiments and thermal modelling of K-feldspars with $^{40}Ar/^{39}Ar$ ages and an evaluation of diffusion parameters of white mica ages reveal white mica neocrystallization related to thrusting at ca. 250-350 °C in quartzite mylonites of the Ruby Gap duplex (central Australia) (Dunlap, 1997). Fossen and Dunlap (1998) found that the eastern part of the basal Caledonian thrust zone under the Jotun Nappe (southern Norway) yielded two age groups: an older (ca. 415-408 Ma) for samples showing thrust-related kinematics, and a younger (ca. 402-394 Ma) for samples reworked by extensional reactivation. Hence, the ages from these samples were interpreted as recrystallization (deformation) ages. In the basement south of the Caledonian nappe front, Mulch and Cosca (2004) demonstrated fluid-assisted synkinematic crystallization of muscovite under temperature conditions of ca. 300 °C during deformation in the Proterozoic Porsgrunn-Kristiansand Shear Zone (southern Norway). Microstructural evidence suggests relatively low temperatures of deformation, whereas homogeneous intragrain $^{40}Ar/^{39}Ar$ and $\delta^{18}O$ data indicate neo- and recrystallization of white mica in the presence of meteoric fluids (Mulch and Cosca, 2004). Comparable results were reported by Mulch et al. (2006) for the Columbia River Detachment (western Canada), based on the lack of correlation between homogeneous $^{40}Ar/^{39}Ar$ apparent ages and effective grain size and microstructural evidence of recrystallization related to dissolution-precipitation, thus suggesting that $^{40}Ar/^{39}Ar$ muscovite ages record neocrystallization and recrystallization in quartzite mylonites. On the other hand, Oriolo et al. (2016b) obtained $^{40}Ar/^{39}Ar$ and K-Ar muscovite and fuchsite data in folded metasediments crosscut by strike-slip shear zones of the Dom Feliciano Belt (central Uruguay). Regional cooling is recorded by foliation-parallel mica ages of ca. 625-600 Ma in metasediments, whereas mica fish in sheared metasediments exhibit ages of ca. 600-580 Ma. Since micas are oriented parallel to the respective metamorphic and mylonitic foliations and the same isotopic systems were evaluated in both folded and sheared metasediments, it can be inferred that recrystallization and strain-related processes during shearing favored isotopic exchange, resulting in ages of sheared rocks that are younger than those of their non-sheared counterparts.

Similarly to Ar, the Rb-Sr system is also likely to be significantly affected by low-T deformation processes. Eberlei et al. (2015) found that mean Rb-Sr muscovite–whole-rock apparent ages decrease from weakly deformed to mylonitic samples that show significant compositional changes along muscovite kink bands, microcracks and subgrain boundaries. These recrystallization-related microstructures constituted diffusion pathways that favored loss of Sr in white micas, suggesting that diffusion in the Rb-Sr system at < 500 °C is controlled by deformation (Eberlei et al., 2015). This is in good agreement with Freeman et al. (1997), who concluded that dynamic (re)crystallization was the main controlling factor for Sr isotopic exchange below closure temperature conditions in mylonites of the Entrelor Shear Zone (northern Italy). Comparable results were obtained by Bozkurt et al. (2011) for the Simav extensional detachment fault zone (Turkey), for which Rb-Sr muscovite and biotite ages seem to record fluid-assisted low-T deformation in mylonites and foliated cataclasites.

In addition to Ar and Sr diffusion in micas, strain- and fluid-related processes can significantly influence isotopic exchange in high temperature thermochronometers, i.e., those yielding closure temperatures above ca. 600 °C (Table 1). Zircon shows the highest closure temperature for the U-Th-Pb system (Table 1; Dahl, 1997; Lee et al., 1997; Cherniak and Watson, 2000), which, nonetheless, can be affected by low-temperature hydrothermal fluids (Geisler et al., 2017; Harley et al., 2007). Re-equilibration of zircon might occur essentially by diffusion-reaction or coupled dissolution-reprecipitation processes, mostly in the presence of fluids (e.g., Mezger and Krogstad, 1997; Geisler et al., 2017). The latter mechanism was reported for mylonites of the Monte Rosa granitic gneiss deformed at ca. 500 °C (Dempster et al., 2008). On the other hand, recent electron backscatter diffraction (EBSD) data from zircons hosted by a strike-slip shear zone in the Eastern Alps (Austria) revealed that zircon may undergo crystal-plastic deformation under amphibolite facies, which in turn may affect element diffusion and zircon geochronology (Kovaleva et al., 2018). Furthermore, weighted Burgers vectors data of MacDonald et al. (2013) indicate that shear zone-related zircons underwent post-crystallization crystal lattice distortion due to plastic deformation, which also modified zircon trace element composition and U-Th-Pb system, since crystal defects provide effective pathways for cation exchange (Reddy et al., 2006).

As in the case of zircon, U-Pb titanite ages may also record the timing of deformation and metamorphism below T_c (Table 1). Oriolo et al. (2016b) obtained a U-Pb LA-ICP-MS concordant titanite age of 588.0 ± 7.1 Ma for mylonites recording sinistral shearing at ca. 550-450 °C along the Sarandí del Yí Shear Zone (Uruguay, Fig. 3a). For the same sample, a U-Pb LA-ICP-MS concordant zircon age of 2048.3 ± 11.0 Ma constrains the timing of the igneous protolith crystallization (Fig. 3b; Oriolo et al., 2016a). Since the titanite age is, within error, comparable to $^{40}Ar/^{39}Ar$ hornblende (Fig. 3c) and muscovite plateau ages of the shear zone recording shear zone deformation (Oriolo et al., 2016a), it might reflect re-equilibration of the U-Th-Pb system during shearing below T_c temperature conditions. In addition, a few titanite ages around 2.0 Ga, which are comparable to the zircon age, record the protolith age (Fig. 3a).

Monazite has a very high closure temperature due to its very low diffusion rates for Th, U and Pb (Table 1; Dahl, 1997; Cherniak et al., 2004; Cocherie et al., 2005; Dahl et al., 2005). When crystallized from granitic melts, monazite can be considered as a highly refractory mineral, but in contrast to zircon, inherited monazite is rarely found in granitoids. In granitoids, the occurrence of magmatic monazite is restricted to peraluminous types, such as two-mica and cordierite-bearing granitoids (Barbarin, 1999). Depending on bulk rock compositions, metamorphic monazite potentially crystallizes in Ca-poor and Al-rich metapelites at temperatures above 300 °C (Spear and Pyle, 2002; Janots et al., 2007; Spear, 2010). Apart from rock bulk composition and metamorphic temperature at medium to low pressures, the (re)crystallization of monazite is apparently controlled by the presence of various fluids, as has been documented in field and experimental studies (McFarlane and Harrison, 2006; Just et al., 2010; Budzyń et al., 2011, 2015, 2017; Harlov et al., 2011; Williams et al., 2011; Schulz and Schüssler, 2013; Harlov, 2015). As a consequence, the Th-U-Pb dating of monazite has a significant potential to constrain geological events in shear zones and the involved protoliths, even below T_c.

Monazite Th-U-Pb dating is based on the observation that concentrations of common Pb in monazite are negligible when compared to radiogenic Pb resulting from the decay of Th and U. As Th concentrations in magmatic and metamorphic monazites are commonly high (ca. 3-14 wt. %), a sufficient amount of radiogenic Pb, detectable by electron microprobe analysis, can accumulate in monazite within a time span of more than ca. 80 my. When the Pb concentrations are near the detection limits, a considerable error arises on the ages (Jercinovic et al., 2008; Montel et al., 1996; Pyle et al., 2005; Suzuki and Kato, 2008; Williams et al., 2006) and, therefore, the age resolution of the method is limited in young orogens. In shear zones within Paleozoic and older orogens, monazite ages can record a polyphase evolution with several age generations below T_c conditions and even involving the protolith history (Shaw et al., 2001; Tchato et al., 2009; Just et al., 2010). For instance, Oyhantçabal et al. (2012) reported identical K-Ar muscovite and Th-U-Pb monazite ages of 606 ± 10 Ma (Fig. 4a, c) for mylonites deformed under greenschist facies conditions (ca. 400-450 °C) in the Rivera Shear Zone (northern Uruguay), clearly below the expected closure temperature of monazite (> 900 °C, Table 1). An older

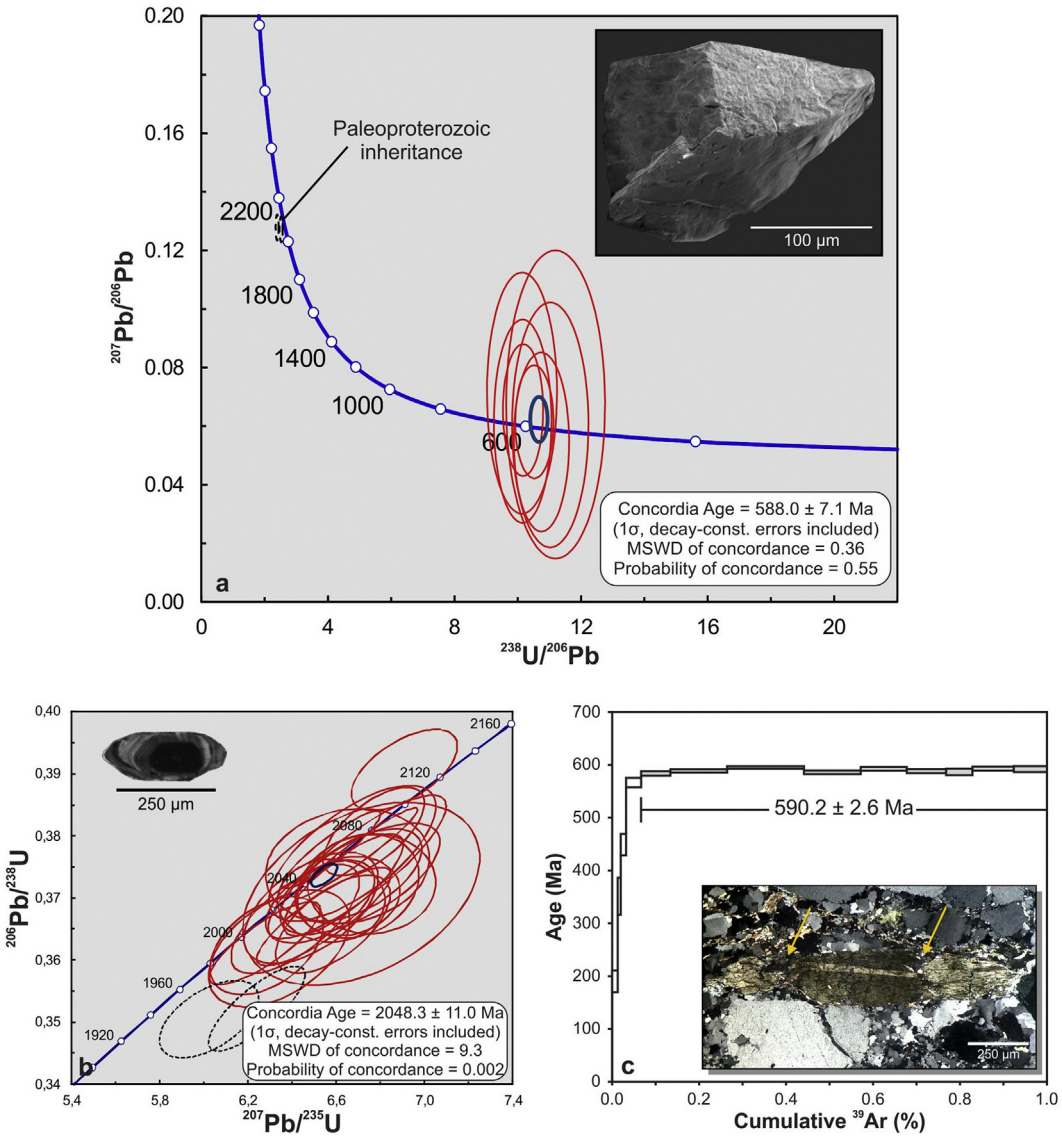

Fig. 3. Geochronologic data of mylonites of the Sarandí del Yí Shear Zone showing resetting of U-Pb titanite ages below T_c conditions during sinistral shearing. The Sarandí del Yí Shear Zone recorded sinistral shearing at ca. 450-550 °C constrained by microstructural and textural data (Oriolo et al., 2015) and a cooling rate higher than 10 °C·my^{-1} (Oriolo et al., 2016a). Closure temperature for Pb diffusion in titanite is above ca. 600 °C, particularly for grain sizes larger than 100 µm (see Fig. 8 for comparison) and cooling rates higher than 10 °C·my^{-1} (Table 1; Cherniak, 1993; Dahl, 1997; Frost et al., 2000). a) U-Pb LA-ICP-MS titanite data (modified after Oriolo et al., 2016b). Paleoproterozoic inheritance is recorded by few crystals, being similar to the protolith age (b), whereas the concordia age defined by most grains is comparable to the Ediacaran $^{40}Ar/^{39}Ar$ hornblende age resulting from sinistral shearing (c). Inset shows SEM micrograph of a representative titanite crystal. b) Paleoproterozoic protolith age recorded by concordant U-Pb LA-ICP-MS zircon data (modified after Oriolo et al., 2016a). Representative cathodoluminiscence image of zircon exhibiting magmatic oscillatory zoning is presented in the inset. c) Timing of sinistral shearing constrained by an $^{40}Ar/^{39}Ar$ hornblende plateau age (modified after Oriolo et al., 2016a). Boudinage of hornblende parallel to the stretching lineation direction is shown in the inset, supporting synkinematic deformation. Arrows indicate interboudin areas.

monazite population, however, also constrains a Paleoproterozoic amphibolite facies metamorphic event at ca. 1.98 Ga (Fig. 4b), succeeding multistage magmatism and high-grade metamorphism at ca. 2.2-2.0 Ga recorded by U-Pb zircon and titanite ages (Fig. 4a; Santos et al., 2003; Oyhantçabal et al., 2012; Oriolo et al., 2016c). Despite its relatively high closure temperature (Table 1), monazite may thus provide temporal constraints in a wide temperature range, covering the spectrum of high- (zircon, titanite) to medium-to-low-temperature (muscovite) thermochronometers.

4. The significance of the protolith

The protolith of mylonitic rocks is typically examined in order to evaluate variations in deformation mechanisms and conditions, and volume-loss reactions (e.g., O'Hara and Blackburn, 1989; Fitz Gerald and Stünitz, 1993; Stipp et al., 2002). In contrast, protoliths have received much less attention in geochronologic studies, in spite of being critical for age interpretations (Oriolo et al., 2016a). At first glance the age of the protolith defines a maximum age for the deformation, which may or may not be useful, depending on the specific case. However, further valuable information might be extracted from a detailed protolith evaluation.

Fig. 5 shows the hypothetic evolution of a shear zone developed in a granitic basement that underwent deformation at t_2 and t_4, assuming that, for instance, t_2 and t_4 shearing events take place at ca. 400 and 300 °C, respectively. Since the granitic protolith I has a crystallization age t_1 that is older than the first deformation event t_2, and t_2 temperature conditions are immediately below the closure temperature for

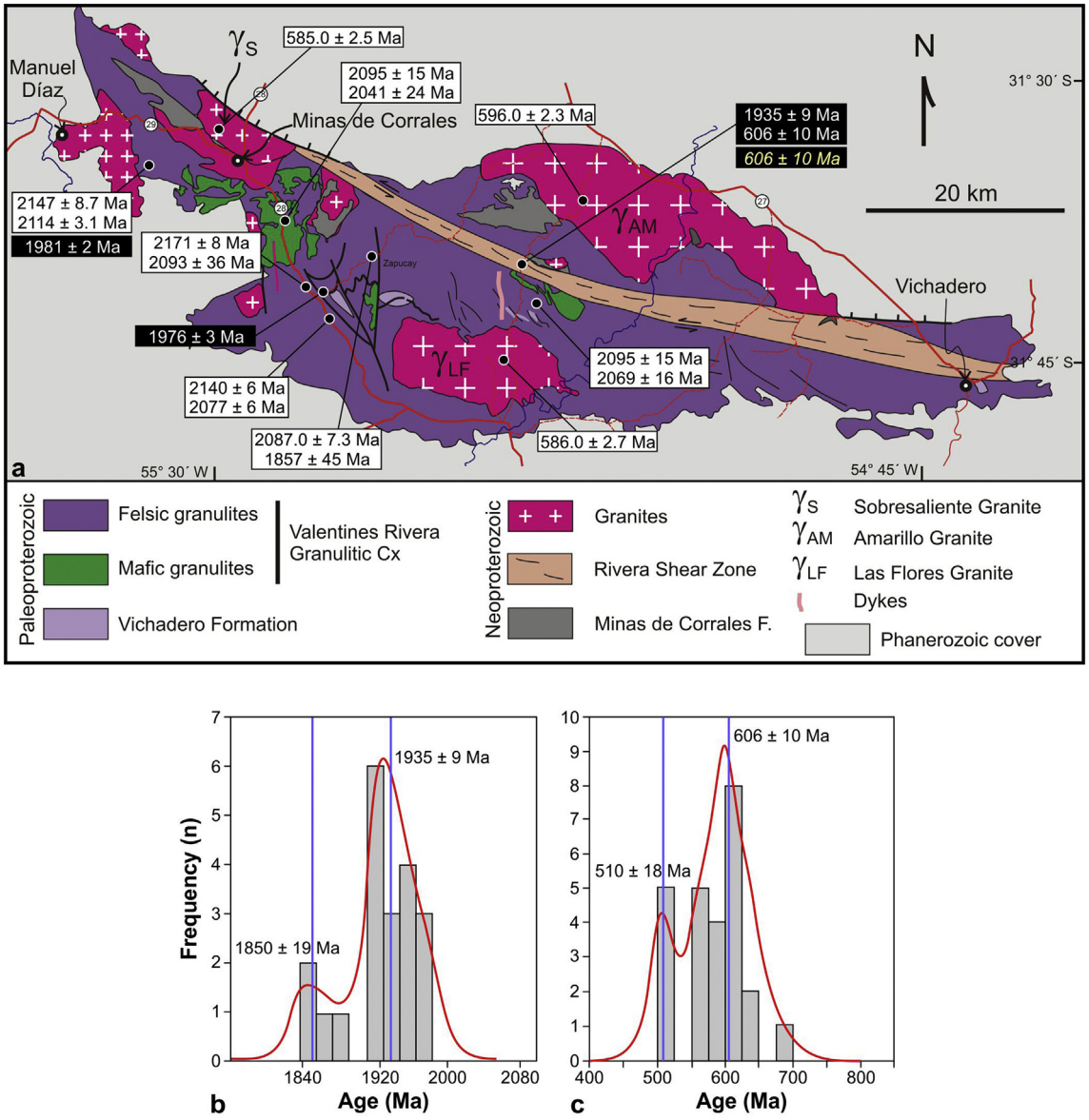

Fig. 4. a) Geological map of the Isla Cristalina de Rivera (Uruguay), where the Rivera Shear Zone is exposed (modified after Oyhantçabal et al., 2012, 2018). Geochronologic data after Santos et al. (2003), Oyhantçabal et al. (2012) and Oriolo et al. (2016c). Zircon U-Pb ages (white rectangles) constrain Paleoproterozoic magmatism and associated high-grade metamorphism, and subsequent Neoproterozoic magmatism. In the Rivera Shear Zone Monazite, Th-U-Pb ages (black rectangles, white text) record both retrograde Paleoproterozoic metamorphism, similar to ages recorded in the Paleoproterozoic Valentines-Rivera Granulitic Complex, and late Neoproterozoic shearing, exactly matching the K-Ar muscovite age (black rectangle, yellow italic text). Record of both Paleoproterozoic (b) and Ediacaran (c) tectonometamorphic events is also illustrated by histograms of monazite ages of the Rivera Shear Zone with distribution function of Sambridge and Compston (1994) (modified after Oyhantçabal et al., 2012). (For interpretation of the references to colour in this figure legend, the reader is referred to the web version of this article.)

Ar diffusion in muscovite, the timing of this event should be recorded by a K-Ar muscovite age obtained from mylonites with this protolith. Conversely, mylonites with a granitic protolith II would not record any deformation prior to t_3 and, hence, no cooling age would predate the timing of protolith crystallization. This means that, for these mylonites, K-Ar muscovite ages may record synkinematic crystallization during t_4 but do not reflect the true thermal history of the shear zone. In other words, true cooling paths can only be obtained from mylonites derived from protolith I, which record the whole T-ε-t evolution of the structure.

An additional problem that may be introduced by intrusions is the resetting of thermochronometers due to contact metamorphism (e.g., Siegesmund et al., 2004; Ayers et al., 2006). Within this framework, the intrusion of granite II may also locally affect thermochronometers in mylonites with the granitic protolith I close to the pluton. In the case of synkinematic intrusions, the expected exponential temperature-distance function for an undisturbed aureole may be replaced by a linear function, since strain may also influence the cooling pattern (Stipp et al., 2004).

The example of Fig. 5 illustrates the importance of understanding protoliths in mylonitic rocks, which is not trivial as deformation may obliterate primary features, particularly when different protoliths are lithologically similar. This was clearly shown for the Sarandí del Yí Shear Zone (Uruguay), which is dominated by granitic mylonites, formed by shearing of ca. 2.1-2.0 Ga granitoids (Oriolo et al., 2015). First, coupled U-Pb and Lu-Hf zircon data allowed the recognition of the Paleoproterozoic wall rock (Oriolo et al., 2016a), since both adjacent blocks (i.e., the Piedra Alta and Nico Pérez terranes) present similar

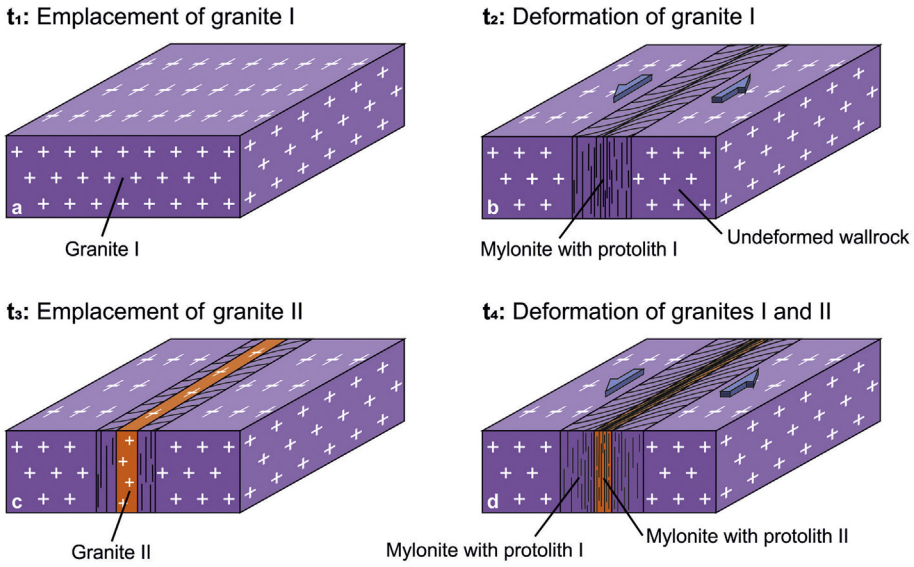

Fig. 5. Example showing the hypothetic evolution of a shear zone with two granitic protoliths. a) Emplacement and crystallization of the granite I at t_1. b) Onset of shear zone deformation at t_2. c) Emplacement and crystallization of the granite II within the shear zone at t_3. d) Final shearing at t_4. Note that only those mylonites with the granitic protolith I would allow reconstructing real T-ε-t paths for the shear zone, since mylonites with the granitic protolith II would not record any event prior to t_3.

zircon crystallization ages but distinct Lu-Hf signatures (Oriolo et al., 2016c). In a broad sense, Lu-Hf signatures permit to distinguish magmas characterized by juvenile depleted-mantle sources (suprachondritic ε_{Hf} values) from those dominated by reworking of older crustal sources (subchondritic ε_{Hf} values), allowing to discriminate between zircon populations that may yield comparable crystallization ages. Paleoproterozoic zircons of the Piedra Alta Terrane and mylonites yield suprachondritic ε_{Hf} values, thus contrasting with coeval zircons of the Nico Pérez Terrane that yield subchondritic ε_{Hf} values (Oriolo et al., 2016a, 2016c). In addition, a second group of granitic protoliths yielded crystallization ages of ca. 0.6 Ga, which are absent in the undeformed wall rock and are coeval with deformation (Oriolo et al., 2016a). These Ediacaran granitic protoliths were thus essential for the evaluation of U-Pb titanite and $^{40}Ar/^{39}Ar$ hornblende and muscovite data (Oriolo et al., 2016a, 2016b), since they are problematic for obtaining true cooling paths (Oriolo et al., 2016a).

In a similar way, a $^{40}Ar/^{39}Ar$ muscovite plateau and U-Pb zircon concordant ages of 585.8 ± 1.6 and 551.0 ± 4.4 Ma, respectively, were obtained for mylonites of the Sierra Ballena Shear Zone (Uruguay) (Oyhantçabal et al., 2010, 2011a). These results may seem contradictory if only closure temperatures for both isotopic systems are considered (Table 1). However, detailed mapping, microstructural analysis and geochemical data reveal that the protolith of the zircon sample corresponds to a rhyolitic dike (Fig. 6) that intruded the shear zone after the onset of deformation, as recorded by its muscovite age, and was subsequently sheared (Oyhantçabal et al., 2010, 2011a).

As in the case of igneous protoliths, ages of mylonites deriving from sedimentary protoliths have to be carefully evaluated, due to possible mixing of metamorphic and detrital ages (e.g.; Kirschner et al., 1996; Dunlap, 1997). In the Western Alps, Villa et al. (2014) interpreted $^{40}Ar/^{39}Ar$ white mica ages as the result of mixing of different mica generations (i.e., detrital, HP metamorphic and shearing-related). According to these authors, Ar inheritance in incompletely recrystallized detrital white mica crystals might thus satisfactorily account for previously reported older ages for the HP event (Villa et al., 2014, and references therein).

5. The brittle-ductile transition

Crustal deformation at depths below or above the brittle-ductile (brittle-plastic) transition has been treated separately in most thermochronologic studies. Methods presented in Table 1 are essentially applicable to ductile shear zones, linked to dynamic recrystallization processes under low- to high-grade metamorphic conditions. In contrast, frictional deformation mechanisms operate in the field of brittle deformation and, therefore, other methods such as K-Ar in illite, feldspar and pseudotachylite, and (U-Th)/He and fission tracks in both apatite and zircon have been applied (e.g., Crone and Omdahl, 1987; Sherlock and Hetzel, 2001; Streepey et al., 2002; Reiners and Brandon, 2006; Whitmeyer, 2008; Cassata et al., 2009; Carrapa, 2010; Löbens et al., 2011, 2017; Wolff et al., 2012; Bense et al., 2014, 2017; Viola et al., 2016; Süssenberger et al., 2017). On the other hand, shear zones recording deformation under conditions close to those of the brittle-ductile transition (ca. 300 ± 50 °C for quartz-rich rocks; e.g., Stipp et al., 2002) typically encompass a complex lithological association including ultramylonites, non-foliated and foliated cataclasites, pseudotachylites, phyllonites, and breccias (e.g.; Sibson, 1977, 1983; Simpson, 1986), thus sharing features of both ductile and brittle deformation. Distinct mineral reactions and deformation mechanisms together with processes such as hydrolytic weakening occur under these conditions, triggering major rheologic changes (Simpson, 1986; Wiberley, 1999; Gueydan et al., 2004; Jefferies et al., 2006; Mancktelow, 2006; Bokuvská et al., 2016). In addition, there is a strong coupling between fluids and deformation at brittle-ductile transition conditions, since deformation may affect permeability and, consequently, fluid flow, which in turn may influence the seismic cycle (e.g., Doglioni et al., 2014; Violay et al., 2017). The seismic cycle, on the other hand, controls upper crustal exhumation, uplift and erosion, thus being intimately related to thermochronology. For this reason, the application of thermochronology in rocks recording shearing at the brittle-ductile transition, so far poorly explored, is evaluated separately in this work.

At first glance, K-Ar ($^{40}Ar/^{39}Ar$) and Rb-Sr biotite seem to be the only methods in Table 1 that are applicable for conditions of ca. 350-300 °C (Fig. 1d). However, both methods can be problematic, since composition and fluids play a major role (Section 3; Jenkin, 1997; Bozkurt et al., 2011; Harrison et al., 1985; Grove and Harrison, 1996; Braun et al., 2006). In addition, biotite is frequently replaced by chlorite under low- to very low-grade conditions (Parry and Downey, 1982; Eggleton and Banfield, 1985) and is more susceptible to Ar and Sr loss than muscovite (Dahl, 1996), thus preventing massive application of these methods to brittle-ductile shear zones. Nevertheless, some contributions show robust $^{40}Ar/^{39}Ar$ biotite ages obtained from ultramylonites recording brittle-ductile deformation (e.g., Whitmeyer, 2008). Since ultramylonites are fine-grained, they pose an analytical challenge for isotopic dating and, therefore, *in situ* or microsampling techniques ($^{40}Ar/^{39}Ar$, Rb-Sr) may be the most adequate tools (e.g., Müller et al., 2000a, 2000b; see also Section 2). On the other hand, K-Ar

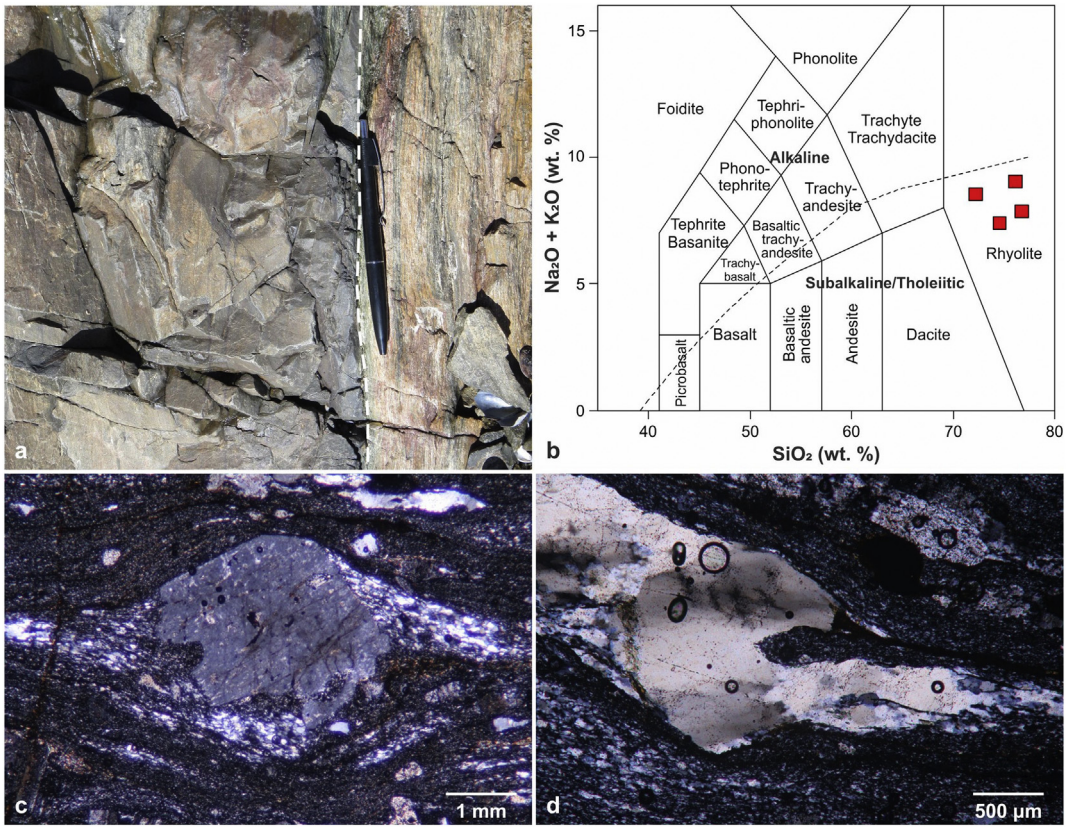

Fig. 6. Compilation of field, geochemical and microstructural evidence documenting the presence of rhyolitic dike intrusion in the Sierra Ballena Shear Zone, Uruguay. See Section 4 for further discussion. a) Field relationships between porphyritic (left) and granitic (right) mylonites (modified after Oriolo et al., 2018). b) Total alkali vs silica diagram (TAS, Le Bas et al., 1986) with geochemical data of porphyritic mylonites, showing their rhyolitic composition (data after Oyhantçabal et al., 2011a). c) Photomicrographs (cross-polarized light) showing K-feldspar porphyroclast (relict phenocryst) in porphyritic mylonite. d) Photomicrographs (cross-polarized light) showing quartz porphyroclast (relict phenocryst) with engulfment in porphyritic mylonite (modified after Oyhantçabal et al., 2010).

and $^{40}Ar/^{39}Ar$ ages can also be obtained for the matrix of pseudotachylites, though the presence of extraneous Ar derived from clasts may lead to geologically meaningless ages (Di Vincenzo et al., 2004).

Alternatively, several contributions have highlighted the potentiality of K-Ar fine mineral fraction ages of white mica to assess the timing of brittle-ductile deformation (e.g., Hunziker et al., 1986; Wemmer and Ahrendt, 1997; Wemmer et al., 2011; Doublier et al., 2015; Hueck et al., 2017; Maffini et al., 2017), although the closure temperature for this system is poorly constrained. Hunziker et al. (1986) indicated a closure temperature for white mica < 2 μm of 260 ± 30 °C. However, data from the KTB (German Continental Deep Drilling Program) borehole showed that *in situ* temperatures of ca. 270 °C are not high enough to reset Cretaceous K-Ar fine fraction ages < 2 μm (Wemmer and Ahrendt, 1997) and, thus, a closure temperature between 275-350 °C seems more likely (Wemmer et al., 2011).

Calculations considering muscovite parameters E_a = 267.8 kJ·mol^{-1} and D_0 = 20 cm^2·s^{-1} (Harrison et al., 2009) suggest closure temperatures of ca. 240-335 °C and 270-360 °C for fine-grained white mica fractions of 0.4-2 μm and 2-6 μm, respectively, and cooling rates between 0.1 and 100 °C·my^{-1} (Fig. 7). However, D_0 = 20 cm^2·s^{-1} is valid for a pressure of ca. 5 kbar (Harrison et al., 2009), which is unrealistic for brittle-ductile transition conditions. According to KTB data (Wemmer and Ahrendt, 1997), a depth of ca. 10 km would approximately coincide with the 300 °C isotherm, which can be assumed to be the mean temperature value of the brittle-ductile transition. At depths of ca. 10 km, a more likely pressure of ca. 2 kbar is to be expected, for which Ar diffusion parameters should be thus recalculated. Following the approach of Harrison et al. (2009), a pressure difference of 3 kbar (from 5 to 2 kbar) would result in an increase of D_0 of a factor of three

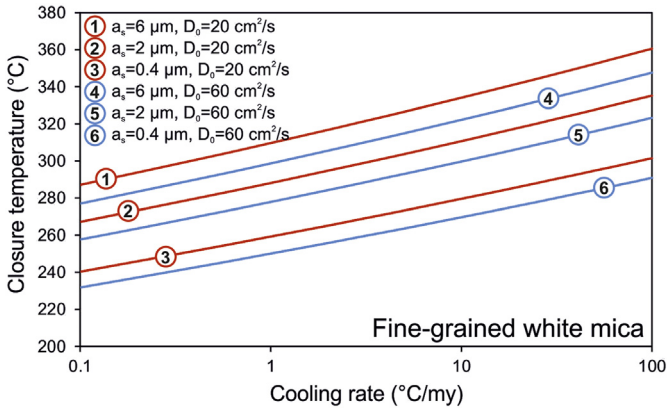

Fig. 7. Variation of closure temperature as a function of cooling rate and effective diffusion radius (a_s) for fine-grained white mica (E_a = 267.8 kJ·mol^{-1}, Harrison et al., 2009). Calculations based on different frequency factor values for pressures of 5 (D_0 = 20 cm^2·s^{-1}, red curves, Harrison et al., 2009) and 2 kbar (D_0 = 60 cm^2·s^{-1}, blue curves) are shown. Closure temperatures were calculated using Closure 1.2 (Brandon et al., 1998; Brandon, 2007). See Section 5 for further details. (For interpretation of the references to colour in this figure legend, the reader is referred to the web version of this article.)

(i.e., 60 cm^2·s^{-1}) relative to that at 5 kbar (i.e., 20 cm^2·s^{-1}). Resulting closure temperatures are only slightly different, with values of ca. 230-325 °C and 260-350 °C for grain size fractions of 0.4-2 μm and 2-6 μm, respectively (Fig. 7).

Calculated closure temperatures are in agreement with data of the KTB borehole (Wemmer and Ahrendt, 1997) and outlines the strong

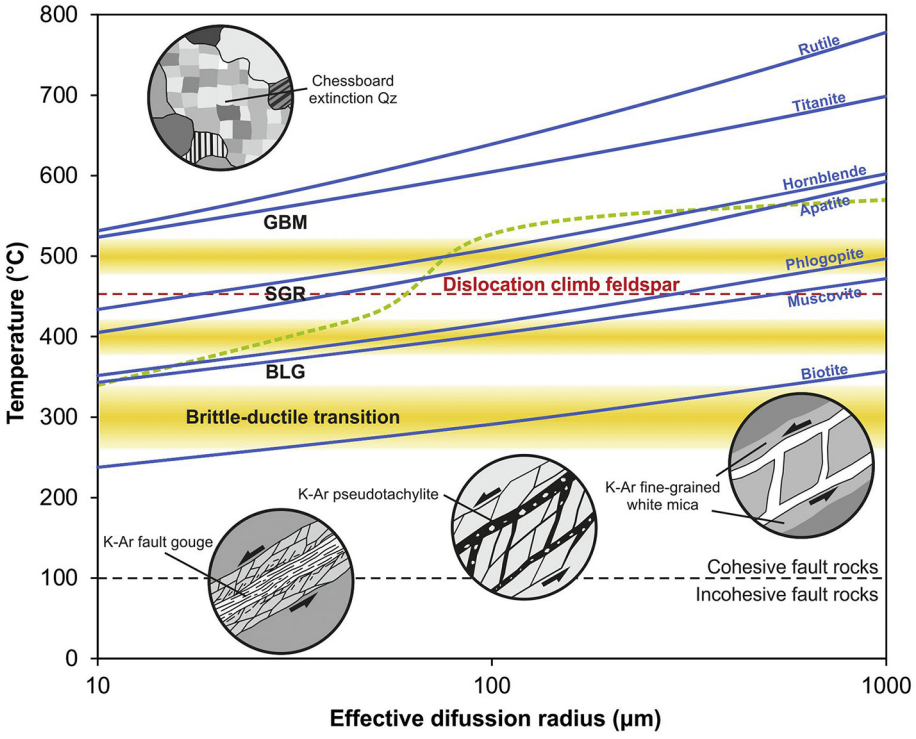

Fig. 8. Compilation of Pb and Ar diffusion data of different minerals used in thermochronology for a cooling rate of 10 °C·my^{-1} and common microstructural proxies of deformation conditions. Pb diffusion data (rutile, titanite, apatite) after Cherniak et al. (2004) and references therein. Note that zircon and monazite are not included due to higher closure temperatures for Pb diffusion (T_c > 900 °C; Dahl, 1997; Lee et al., 1997; Cherniak and Watson, 2000; Cherniak et al., 2004). Ar diffusion data recalculated using Closure 1.2 (Brandon et al., 1998; Brandon, 2007), considering selected parameters of Fig. 1 (hornblende: E_a = 268 kJ·mol^{-1}, D_0 = 0.024 cm^2·s^{-1}, Harrison, 1981; phlogopite: E_a = 242 kJ·mol^{-1}, D_0 = 0.075 cm^2·s^{-1}, Giletti, 1974; muscovite: E_a = 267.8 kJ·mol^{-1}, D_0 = 20 cm^2·s^{-1}, Harrison et al., 2009; biotite: E_a = 197 kJ·mol^{-1}, D_0 = 0.075 cm^2·s^{-1}, Harrison et al., 1985; Grove and Harrison, 1996). For temperature conditions close to or below brittle-ductile transition conditions (ca. 300 °C), isotopic systems and methods are schematically shown (K-Ar or ^{40}Ar/^{39}Ar fine-grained white mica data in phyllonites, ultramylonites or sericitic alteration halos associated with ore-bearing brittle-ductile structures; K-Ar pseudotachylite; and K-Ar fault gouge). Quartz dynamic recrystallization mechanisms and transitional fields (yellow) after Stipp et al. (2002). BLG: bulging recrystallization, SGR: subgrain rotation recrystallization, GBM: grain boundary migration recrystallization. In the GBM field (Stipp et al., 2002), quartz chessboard extinction is observed at temperatures from ca. 600 to 800 °C at ca. 1 to 9 kbar, respectively (Kruhl, 1996). Mean grain size of dynamically recrystallized quartz crystals is illustrated by the green curve (modified after Stipp et al., 2002). Onset of dislocation climb in feldspars after Pryer (1993). Approximate boundary between cohesive and incohesive fault zone rocks after Sibson (1983). See text for further discussion.

potential of K-Ar fine fraction white mica geochronologic studies for shear zones recording deformation close to brittle-ductile transition conditions. Moreover, the combination of K-Ar dating with XRD data allows the quantification of the crystallinity index (Kübler Index), which is useful in order to assess temperature conditions and to discriminate between neoformed and inherited crystals (e.g., Löbens et al., 2011; Wemmer et al., 2011; Doublier et al., 2015). This can be particularly useful in fine-grained white mica-rich rocks such as ultramylonites and phyllonites (Jefferies et al., 2006), and also in ore-bearing brittle-ductile shear zones (Deckart et al., 2005; Harbi et al., 2017; Maffini et al., 2017), which commonly exhibit associated hydrothermal sericite (e.g.; Zhu et al., 2011).

6. Discussion

6.1. Isotopic closure and deformation

Since shear zones result from a complex interplay of deformation, metamorphism and/or associated fluids, active relationships between deformation and metamorphism (Williams and Jercinovic, 2012) must be understood for a correct interpretation of geochronologic data (Villa, 1998). Active relationships imply a direct coupling between these processes (Williams and Jercinovic, 2012), among which one of the most important interactions is the role that deformation plays in promoting the removal of unstable phases and the growth of new stable phases (Marsh et al., 2009; Goncalves et al., 2012; Williams and Jercinovic, 2012). A good example is synkinematic recrystallization, which results from a combination of dynamic recrystallization and metamorphic reactions (Yund and Tullis, 1991; Stünitz, 1998). Moreover, strain localization and/or changes in deformation mechanisms can strongly influence reaction rates and kinetic pathways in high strain contexts (Mulch et al., 2002; Cosca et al., 2011), in contrast to regional metamorphism, where diffusion and resulting reaction rates vary as a function of temperature (Steffen and Selverstone, 2006). For instance, localized fluid-assisted deformation gives rise to mylonite development and, consequently, creates a chemical potential gradient between the thermodynamically metastable undeformed wall rock and the mylonitic belt (Goncalves et al., 2012). This chemical gradient, in turn, drives further reactions and mass transfer processes (Goncalves et al., 2012).

In order to provide robust P-T-ε-t paths of shear zones, geochronologic data need thus to be combined with independent P-T estimates and microstructural and/or textural data constraining mineral deformation mechanisms and inferred deformation conditions (e.g., Steffen and Selverstone, 2006; Forster and Lister, 2009; Cosca, 2013; Villa et al., 2014; Gasser et al., 2015; Oriolo et al., 2016a). As an example, Fig. 8 shows closure temperatures for Pb and Ar diffusion in different minerals as a function of the effective diffusion radius combined with commonly used microstructural proxies to constrain deformation conditions, such as quartz and feldspar microstructures and deformation mechanisms (Kruhl, 1996; Stipp et al., 2002). In the case of monazite, for example, deformation mechanisms play a major role in the U-Th-Pb system (e.g., Wawrzenitz et al., 2012). Feldspar-rich layers governed by feldspar dislocation climb (Fig. 8) are more likely to host monazites that record the pre-mylonitic history, whereas those dominated by dissolution-precipitation processes, such as those recording feldspar-to-muscovite reaction (Wiberley, 1999), may exhibit synkinematic monazites that yield ages related to the mylonitic event (Wawrzenitz et al., 2012). In layers dominated by dissolution-precipitation, an increase in the alkali content favors a higher reactivity of the fluid, which in turn leads to dissolution of old monazite grains and nucleation of new synkinematic crystals (Wawrzenitz et al., 2012). On the other hand, deformation mechanisms also play a major role in isotopic diffusion in quartz (O'Hara et al., 1997, and references therein), though their implications for geochronology have been so far poorly explored. Based on natural shear zone data, Kirschner et al. (1995) and O'Hara et al. (1997) proposed that dynamic recrystallization, particularly when related to grain boundary migration, triggers oxygen isotopic exchange in quartz, which can be used to constrain

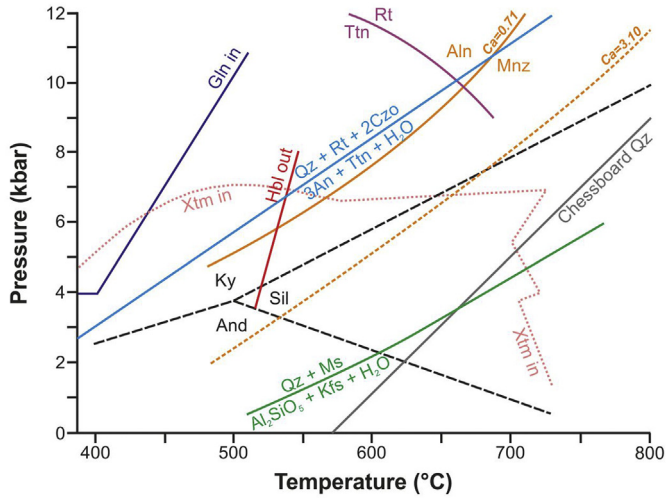

Fig. 9. P-T conditions for some metamorphic reactions involving minerals used in thermochronology. Lower stability limit of hornblende (red) in mafic rocks after Apted and Liou (1983). Rutile-titanite equilibrium (violet) for Ca-rich (ca. 3 wt. % of CaO) metagranitoids after Angiboust and Harlov (2017). Qz + Rt + 2Czo = 3An + Ttn + H_2O equilibrium (light blue) in mafic rocks after Kapp et al. (2009). Qz + Ms = Al_2SiO_5 + Kfs + H_2O equilibrium (green) after Haselton Jr. et al. (1995). Stability fields of monazite and allanite at different bulk rock contents as a function of Ca molar content (bold orange line: Ca = 0.71; dashed orange line: Ca = 3.10), together with the xenotime stability field (Janots et al., 2007; Spear, 2010). Lower limit for the appearance of chessboard extinction in quartz (grey) after Kruhl (1996) is also shown. Qz: quartz, Rt: rutile, Czo: clinozoisite, An: anortite, Ttn: titanite, Hbl: hornblende, Ms: muscovite, Kfs: K-feldspar, Ky: kyanite, Sil: sillimanite, And: andalusite, Mnz: monazite, Aln: allanite, Xtm: xenotime, Gln: glaucophane. (For interpretation of the references to colour in this figure legend, the reader is referred to the web version of this article.)

temperature deformation conditions. In addition, crystallographic-preferred orientation arising from dynamic recrystallization further promotes oxygen anisotropic diffusion (O'Hara et al., 1997), since diffusion parallel to the c-axis is about two orders of magnitude faster than that normal to it, as shown by experimental data on natural and synthetic samples (Giletti and Yund, 1984). Experimental data of Giletti and Yund (1984) also demonstrated a change in the slope on the Arrhenius plot at the α-β transition, arising from variations of Arrhenius parameters D_0 and E_a for α- and β-quartz. The occurrence of the α-β transformation can be inferred by the presence of chessboard extinction (Fig. 8; Kruhl, 1996; Stipp et al., 2002), which in turn can provide constraints on P-T conditions (Kruhl, 1996).

Concerning metamorphic reactions, those involving minerals used for geochronologic studies are of particular interest (Fig. 9), as they might provide some hints of the coupled P-T and deformation history of the rock (Apted and Liou, 1983; Berger and Stünitz, 1996; Wiberley, 1999; Janots et al., 2007; Kapp et al., 2009; Spear, 2010; Gasser et al., 2015; Angiboust and Harlov, 2017). For instance, mylonitic gneisses of the Central Cameroon Shear Zone (Fig. 10a) show apatite-allanite corona structures around monazite (Fig. 10b, c) that are interpreted to result from monazite decomposition, probably during decreasing pressure and temperature (Finger et al., 1998). The stability fields of monazite and allanite can be further constrained by whole-rock geochemical data, since they vary as a function of Ca contents (Fig. 9). Apatite-allanite coronas can thus be explained by pseudomorphic partial replacement of the original monazite by apatite and allanite via fluid-assisted dissolution-precipitation process (Budzyń et al., 2011; Harlov et al., 2011). Satellite monazite may be present as well (Fig. 10d), though its microstructures have so far been described only by Finger et al. (2016). These monazite satellite grains may crystallize during an increase in temperature after the formation of allanite-apatite coronas surrounding the monazite, thus revealing a period of decreasing and then increasing P-T conditions. Similarly, the formation of

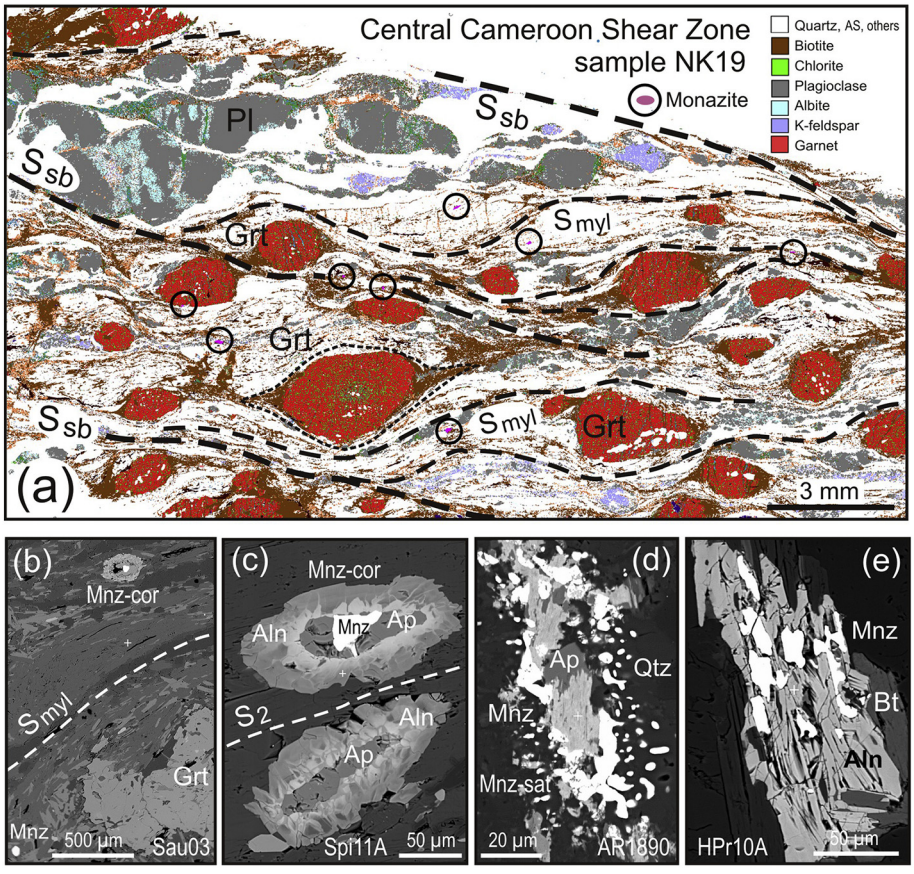

Fig. 10. a) Map of energy-dispersive X-ray (EDX) spectra (GXMAP by automated SEM) from mylonitic garnet gneisses of the Central Cameroon Shear Zone in XZ section parallel to the stretching lineation, as described by Tchato et al. (2009). Zoned garnet porphyroblasts of the protolith are preserved in microlithons surrounded by a fine-grained mylonitic foliation (S_{myl}), which is transected by a shear band foliation (S_{sb}). The spectral mapping allows to identify the location and microstructural features of monazite. b) Lenticular monazite corona structure (Mnz-cor) in a mylonitic garnet gneiss (S_{myl}) with garnet (Grt) and preserved monazite (Mnz) in microlithon; kyanite flasergneiss of the Austroalpine basement (Schulz, 2017). c) Details of the apatite-allanite-monazite (Aln, Ap, Mnz) corona structure in micaschists from the Austroalpine basement. d) Monazite satellite structure (Mnz-sat) with tiny newly formed monazite grains in high temperature mylonitic garnet gneiss of the Alpine External Massive (Schulz and von Raumer, 2011). e) Crystallization of new monazite inside allanite (Aln) in garnet micaschist of the Austroalpine basement (Krenn et al., 2012).

new tiny monazite grains within large allanite porphyroblasts (Fig. 10e) seems to record increasing temperatures across the allanite-monazite univariant reaction (Fig. 9; Janots et al., 2007; Spear, 2010).

Single mineral phases providing constraints on both P-T conditions and timing of shearing may thus be particularly useful, as in the case of amphiboles. Amphibole-bearing mafic igneous rocks and their metamorphic equivalents such as eclogites, blueschists and amphibolites commonly occur as isolated lenses and pods within low- to medium-grade shear zones. Crystallization and recrystallization of sodic, sodic-calcic and calcic amphiboles occurs during shear zone development. The distribution of Si, Al and Na in amphibole crystallographic sites depends on the physical conditions of crystallization, with Si increasing and Al decreasing from hornblende to actinolite compositions at decreasing temperatures. In addition, the lower stability limit of hornblende at ca. 500-550 °C also provides some constraints in the case of mafic protoliths (Fig. 9). Ca-amphibole zonations are best described in terms of ^{IV}Al, ^{VI}Al and Ti, which semiquantitatively monitor the temperature and pressure changes and allow geothermobarometry within amphibolite to lower greenschist facies conditions at intermediate to low pressures (Zenk and Schulz, 2004). When combined with microstructural and K-Ar (^{40}Ar/^{39}Ar) data, the amphibole P-T-ε-t path can be reconstructed in detail. This was exemplified by Stünitz (1998) for shear zones of the Ivrea Zone (northern Italy), which host recrystallized grains of hornblende with lower Al- and Ti-contents than the porphyroclasts, thus recording retrograde P-T conditions during deformation.

Within this framework, development of analytical methods allowing *in situ* measurements may also hold the key to correctly interpret ages in terms of deformation processes and metamorphic reactions. In the case of monazite, for instance, isotopic U-Pb analyses by TIMS, SHRIMP and LA-ICP-MS are of limited application in shear zones due to the required minimum grain size of ca. 50 μm. Smaller grain sizes are hard to extract for grain mounts and hard to detect for such measurements. In this situation, the total Th-U-Pb dating of monazite by the electron microprobe (EMP) provides a unique potential (Suzuki et al., 1991; Montel et al., 1996; Spear et al., 2009). It allows *in situ* analysis of monazite grains with a minimum size of 10 μm in distinct microstructural sites, which can be directly evaluated in terms of specific reaction and deformation microstructures, and in the same thin sections that can be studied by EBSD for textural analysis and/or for geothermobarometry. The EMP Th-U-Pb dating method requires a thorough inspection of the polished thin sections by SEM. First, automated mineralogical methods by SEM (e.g., the mineral liberation analysis, Fandrich et al., 2007; Schulz, 2017) allow finding the location of tiny monazite grains in backscattered images (Fig. 10a). In combination with monazite mineral chemistry (e.g., LREE, Y, Ca, Si, Th, U), these deformation-related and/or reaction microstructures provide irreplaceable information for the geological interpretation of geochronologic data in ductile shear zones (Fig. 10).

Since temperature is clearly not the only variable controlling isotopic systems, particularly in shear zones, isotopic ages of mylonitic rocks should be interpreted in the light of several processes that control isotopic diffusion (e.g.; Dahl, 1996; Dunlap, 1997; Villa, 1998; Mulch and Cosca, 2004; Villa et al., 2014; Oriolo et al., 2016a), among which the most important are:

- Cooling (below T_c)
- Neocrystallization
- Recrystallization
- Interaction with fluids
- Protolith age

The interpretation of cooling ages from thermochronologic data is based on the assumption of thermally activated diffusion, which is not necessarily valid in all cases (Sections 3.3 and 4). Alternatively, isotopic data can be explained as the result of neo- or recrystallization triggered by metamorphic reactions (Fig. 9). One of the most common reactions in granitic mylonites is the fluid-assisted breakdown of K-feldspar and plagioclase to white mica, which may also have a significant influence in strain hardening/softening processes (e.g.; Williams and Dixon, 1982; Wiberley, 1999; Whitmeyer and Wintsch, 2005). Since these reactions occur below ca. 500 °C (Wiberley, 1999), they may overlap with the muscovite closure temperature for Ar (Fig. 1; Harrison et al., 2009), leading to ambiguities in data interpretation, i.e., cooling vs neocrystallization (Dunlap, 1997). In a similar way, dynamic recrystallization is commonly accompanied by metamorphic reactions that may give rise to changes in mineral composition (Yund and Tullis, 1991; Stünitz, 1998) and, hence, different mineral compositions may yield different ages associated with different processes (Di Vincenzo et al., 2001; Mulch and Cosca, 2004). Minor and trace element contents seem thus to be crucial to discriminate age populations, as in the case of monazite, where PbO, ThO_2, Y_2O_3 and UO_2 have been proved to be extremely useful to separate monazite generations related to distinct magmatic, regional metamorphic and mylonitic events (Tchato et al., 2009; Just et al., 2010; Schulz and von Raumer, 2011; Oyhantçabal et al., 2012). Further complications arise from the presence of fluids, which in turn may further promote neo- and recrystallization (e.g.; Wiberley, 1999; Mulch and Cosca, 2004; Bozkurt et al., 2011), and inheritance of the protolith age (Section 4). These phenomena can also lead to geologically meaningless ages, resulting from the presence of an open system or mixing of different age populations, among others.

Therefore, the combined effects of all these factors can only be disentangled by a careful examination of the P-T history, diffusion parameters, mineral composition, reaction microstructures, and deformation mechanisms and conditions (Dunlap, 1997; Di Vincenzo et al., 2001; Mulch and Cosca, 2004; Forster and Lister, 2009; Just et al., 2010; Forster et al., 2014; Villa et al., 2014; Oriolo et al., 2016a; Druguet et al., 2018). In addition, regional to outcrop-scale structural data are crucial to correctly interpret geochronologic data.

6.2. Assessing the timing of shearing

Solid-state deformation-related processes play a major role in the isotopic systems of different minerals in mylonitic rocks and, therefore, age interpretation cannot be only based on a certain T_c value but also needs a detailed evaluation of deformation mechanisms and P-T conditions (Section 6.1). For this reason, a robust reconstruction of the shear zone deformation history needs to combine geochronologic data of pre-, syn- and post-kinematic minerals of mylonites together with further geochronologic constraints on shear zone-related intrusions, protolith age(s) and adjacent blocks (Fig. 11; Section 4; Mezger et al., 1992b; van der Pluijm et al., 1994; Siegesmund et al., 2008; Cosca, 2013; Schneider et al., 2013; Oriolo et al., 2016a).

Intrusions that are spatially related to shear zones are commonly used to provide temporal constraints on shear zone activity, particularly since massive application of U-Pb zircon geochronology, which allows obtaining a relatively precise crystallization age. All, pre-, syn-, inter- and post-kinematic intrusions are of interest, as they provide independent constrains on the timing of shearing. Hence, a detailed analysis of magmatic fabrics (Paterson et al., 1989) is critical to discriminate between pre-, syn- and post-kinematic igneous bodies (Fig. 11), based on either field mapping of magmatic foliations and lineations or anisotropy of magnetic susceptibility data (e.g., Hutton et al., 1990; Brown and Solar, 1998; Paterson et al., 1998; Steenken et al., 2000; Rosenberg, 2004). In particular, intrusions do not only provide constraints on the timing of shear zone activity, but also additional valuable information on kinematics and strain (Ramsay, 1980; Wheeler, 1987; Oyhantçabal et al., 2001; Vitale and Mazzoli, 2010; Lisle, 2014). As shown by Sassier et al. (2009) for the Ailao Shan-Red River Shear Zone (Southeast Asia), coupled strain analysis and U-Pb zircon dating of different generations of syntectonic dikes allow calculation of strain rate. In high-grade metamorphic settings,

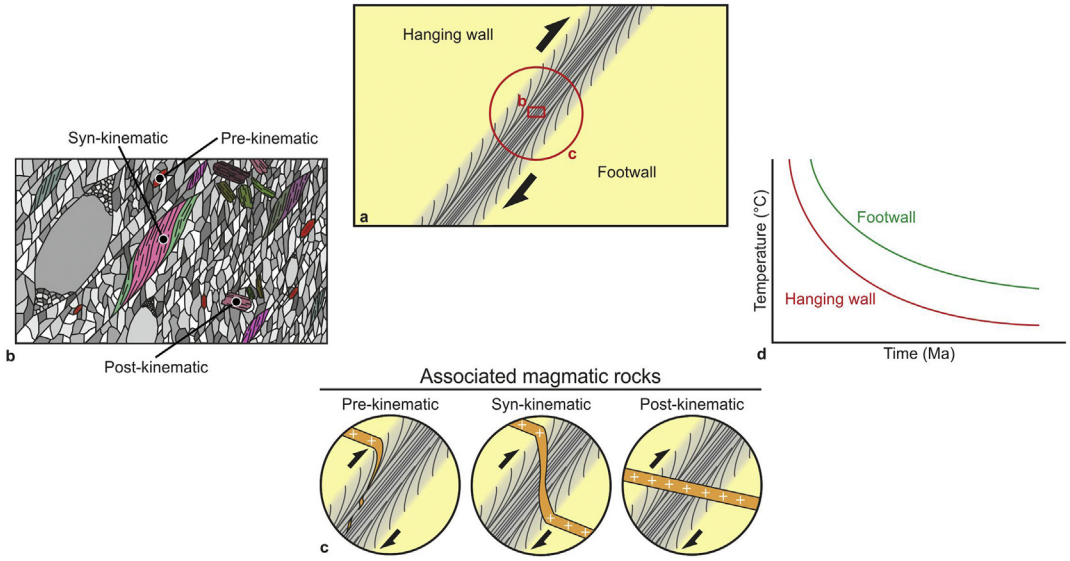

Fig. 11. a) Sketch with different approaches to assess the timing of shear zone activity. b) Dating pre-, syn- and post-kinematic minerals in mylonites. For a hypothetic shear zone deformed under greenschist facies conditions, prismatic zircon, muscovite fish and randomly oriented biotite are schematically presented as pre-, syn- and post-kinematic minerals, respectively. c) Obtaining crystallization ages of associated intrusions. d) Collecting thermochronologic data from adjacent blocks.

crystallization ages of anatectic melts formed during shearing constrain deformation in shear zone-related migmatites (Bhadra et al., 2007; Weinberg and Mark, 2008; Viegas et al., 2013; Carvalho et al., 2016).

On the other hand, thermochronologic data in adjacent blocks are particularly interesting, as they have a great potential to resolve differential cooling and/or exhumation histories along shear zones, which, in turn, can be interpreted in the light of structural and kinematic data (e.g., van der Pluijm et al., 1994; Siegesmund et al., 2008; Oyhantçabal et al., 2009b). Additionally, the thermal stability of different blocks can be assessed (e.g., cratonic vs. metacratonic areas, Black and Liégeois, 1993; Liégeois et al., 2013) and, consequently, the role of shear zones as major crustal thermal boundaries can be evaluated (Oyhantçabal et al., 2011b; Cao and Neubauer, 2016; Oriolo et al., 2016a).

As all these direct and indirect temporal constraints on shear zone activity (Fig. 11) have some limitations and, if considered separately, may lead to ambiguous interpretations (van der Pluijm et al., 1994; Oriolo et al., 2016a), complex shear zone histories should be reconstructed in the light of multiproxies. As an example, geochronologic data of the Sarandí del Yí Shear Zone (Fig. 3; Oriolo et al., 2016a, 2016b) are integrated with information of adjacent blocks and associated intrusions (Fig. 12). In the first place, deflected dikes yielding crystallization ages of ca. 1.79 Ga (Halls et al., 2001) provide a maximum age constraint for shearing (Bossi and Campal, 1992; Oyhantçabal et al., 1993; Oriolo et al., 2015). In this case, however, the maximum age inferred from passive markers does not represent any precise constraint, since shearing is much younger at ca. 0.63-0.58 Ga (Oriolo et al., 2016a, 2016b). On the other hand, the Solís de Mataojo Granitic Complex (584 ± 13 Ma, Pb-Pb titanite stepwise leaching; Oyhantçabal et al., 2007) presents magmatic fabrics that reveal a syn-kinematic emplacement during sinistral shearing of the Sarandí del Yí Shear Zone (Fig. 12a; Oyhantçabal et al., 2001) and, hence, constrain the timing of shearing, which is comparable with the age inferred from thermochronologic data of mylonitic rocks (Fig. 3; Oriolo et al., 2016a, 2016b). A second intrusion, the Cerro Caperuza granite, constrains the end of ductile deformation, as it intrudes the mylonites but shows macroscopically isotropic magmatic fabrics (Fig. 12a; Oriolo et al., 2016a). Zircons of this granite yielded a U-Pb LA-ICP-MS crystallization age of 570.9 ± 11.0 Ma (Fig. 12a; Oriolo et al., 2016a), which is younger than ages recorded in the mylonitic belt (Fig. 3; Oriolo et al., 2016a, 2016b), thus confirming field relationships. Finally, K-Ar muscovite data from adjacent blocks indicate that the Sarandí del Yí Shear Zone represented a major thermal boundary during the late Neoproterozoic Brasiliano–Pan-African orogeny, as it separates a large Paleoproterozoic cratonic domain where Paleoproterozoic K-Ar and ^{40}Ar-^{39}Ar mica ages are preserved (i.e., the Río de la Plata Craton) from a block that was reworked and thermally overprinted during the Ediacaran (i.e., the Nico Pérez Terrane) (Fig. 12b; Oyhantçabal et al., 2011b; Oriolo et al., 2016a).

Though out of the scope of this contribution, this multiproxy approach to assess the timing of shear zone deformation can be easily extrapolated to the brittle field. Direct dating of shear zone rocks by means of K-Ar and/or ^{40}Ar/^{39}Ar data of fine-grained white mica, pseudotachylite and fault gouge (Fig. 8; Parry et al., 2001; Sherlock and Hetzel, 2001; van der Pluijm et al., 2001; Whitmeyer, 2008; Löbens et al., 2011; Wemmer et al., 2011; Tagami, 2012; Bense et al., 2014; Torgersen et al., 2014; van der Pluijm and Hall, 2015; Ksienzyk et al., 2016; Viola et al., 2016; Maffini et al., 2017; Süssenberger et al., 2017) can be combined with thermal modeling of (U-Th)/He and fission tracks in apatite and zircon and/or ^{40}Ar/^{39}Ar feldspar data in adjacent blocks (e.g., Lovera et al., 1989; Streepey et al., 2002; White and Hodges, 2002; Zwingmann and Mancktelow, 2004; Braun et al., 2006; Reiners and Brandon, 2006; Cassata et al., 2009; Carrapa, 2010; Zwingmann et al., 2010; Tagami, 2012; Chew and Spikings, 2015). This integrated focus allows reconstructing the long-term evolution of faults and associated exhumation, uplift and sedimentary processes (e.g., Zwingmann and Mancktelow, 2004; van der Pluijm et al., 2006; Löbens et al., 2011, 2017; Tagami, 2012; Davids et al., 2013; Bense et al., 2014, 2017; Hnat and van der Pluijm, 2014; Fossen et al., 2016; Viola et al., 2016; Hueck et al., 2017; Ring et al., 2017; Süssenberger et al., 2017).

Furthermore, several of the aforementioned aspects can be considered to date non-mylonitic deformation fabrics as well. The timing of metamorphic foliation development, for instance, can be constrained by obtaining ages on syn-metamorphic minerals, as in the case of white mica and illite ages used to date the timing of cleavage development. These minerals may lie parallel to cleavage planes and record local slip along them, or alternatively occur within strain fringes, thus indicating their contemporaneity with cleavage formation (Chan et al., 2000; Sherlock et al., 2003; McWilliams et al., 2007; Wang et al., 2016; Süssenberger et al., 2017). In the case of fold axial plane cleavage, dating of cleavage can be further applied to quantify the age of folding

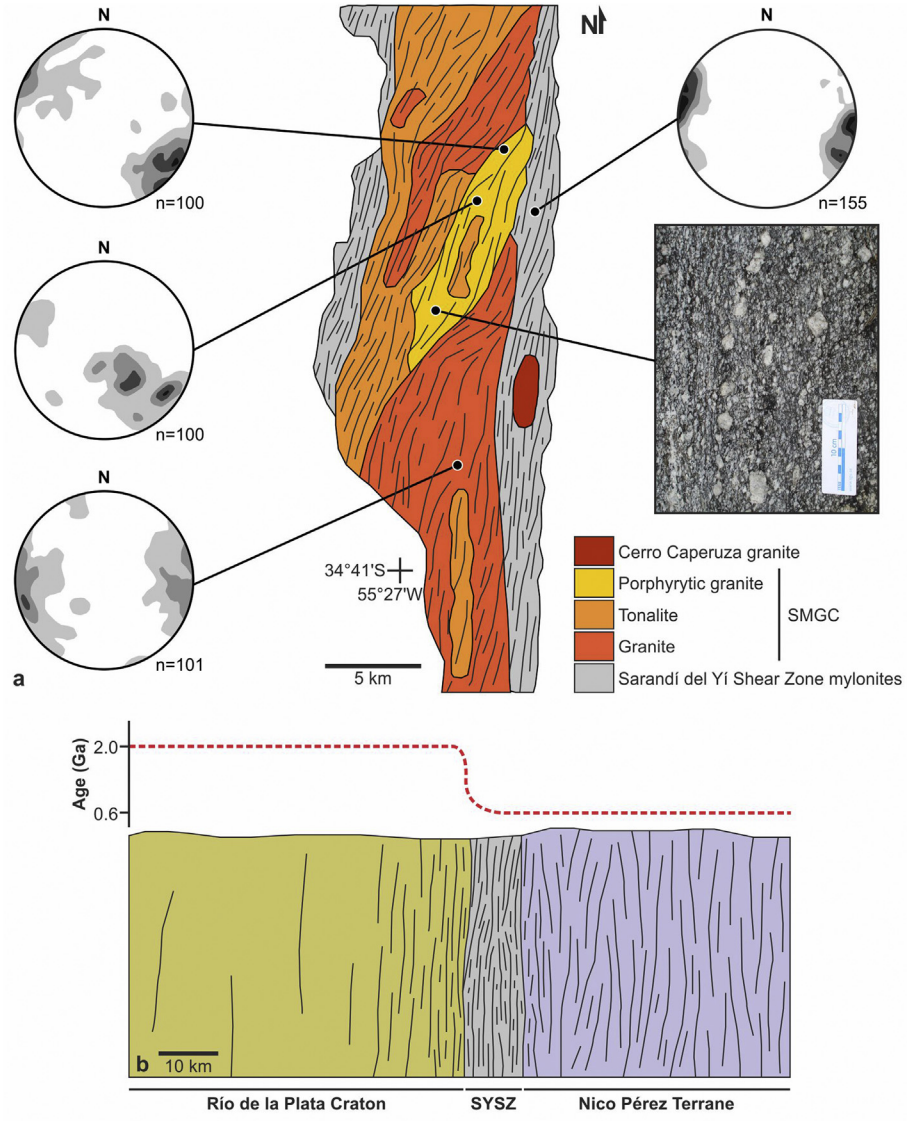

Fig. 12. a) Facies map of the Solís de Mataojo Granitic Complex (SMGC), synkinematically emplaced during sinistral shearing along the Sarandí del Yí Shear Zone (SYSZ) (modified after Oyhantçabal et al., 2001). Lower hemisphere equal area projections of magmatic foliation poles of the SMGC defined by shape-preferred orientation (SPO) of K-feldspar crystals (left) and solid-state mylonitic foliations of the SYSZ (right), which present a similar orientation (Oyhantçabal et al., 2001; Oriolo et al., 2015). The photograph illustrates SPO of K-feldspars in the porphyrytic granite. The SMGC presents an age of 584 ± 13 Ma (Pb-Pb titanite stepwise leaching, Oyhantçabal et al., 2007), which is comparable to U-Pb titanite, and $^{40}Ar/^{39}Ar$ hornblende and muscovite data of the SYSZ of ca. 600-580 Ma (Fig. 3; Oriolo et al., 2016a, 2016b), supporting a synkinematic emplacement. In contrast, the Cerro Caperuza granite presents a crystallization age of 570.9 ± 11.0 Ma (U-PB LA-ICP-MS zircon, Oriolo et al., 2016a), which constrains the end of ductile deformation since the granite lacks in field magmatic fabrics and cross-cut mylonitic fabrics. b) Schematic regional profile showing variation of K-Ar and $^{40}Ar/^{39}Ar$ muscovite ages across the Sarandí del Yí Shear Zone (data after Oyhantçabal et al., 2009b, 2011b; Oriolo et al., 2016a, 2016b). Ages of ca. 2.0-1.8 Ga in the Río de la Plata Craton point to a relative thermal stability during the Neoproterozoic, with only minor evidences of reworking close to the SYSZ (Oriolo et al., 2015, 2016a). In contrast, significant late Neoproterozoic crustal reworking is evidenced by ages of ca. 0.60-0.58 Ga in the Nico Pérez Terrane, which are similar to those of the SYSZ. Note similarities with the model of exhumed metamorphic core complex along major strike-slip shear zones proposed by Cao and Neubauer (2016).

(Fitz-Díaz and van der Pluijm, 2013; Süssenberger et al., 2014; Wang et al., 2016). On the other hand, dating of porphyroblasts, which commonly exhibit microstructures that allow to constrain the timing of one or more generations of metamorphic fabrics (e.g., Johnson, 1999), can also provide robust temporal constraints. In particular, garnet porphyroblasts have been of great interest, since both Sm-Nd and Lu-Hf ages and P-T estimations can be obtained in garnet, even allowing to track complex metamorphic and deformational histories and their timescales based on crystal zonation patterns (Mezger et al., 1992a; Ganguly and Tirone, 1999; Ducea et al., 2003; Caddick et al., 2010; Pollington and Baxter, 2011; Skrzypek et al., 2011; Smit et al., 2013; Cheng et al., 2016).

The integration of geochronologic data of shear zones, associated igneous bodies and adjacent blocks is a powerful tool to disentangle complex deformational histories involving strain partitioning and localization (Fig. 11). In orogens, strain is heterogeneously distributed at all scales, leading to partitioning into different domains of relatively homogeneous strain, which, as a whole, accommodate the total strain (Tikoff and Teyssier, 1994; Jones and Tanner, 1995; Teyssier et al., 1995; Fossen and Tikoff, 1998; Carreras et al., 2013). In addition to these spatial heterogeneities, strain may also vary with time (Lister and Williams, 1983; Hobbs et al., 1990; Platt and Behr, 2011b), which is intrinsically related to strain hardening/softening processes (Vitale and Mazzoli, 2008; Fossen and Cavalcante, 2017). For this reason, field-based geological and structural observations at different scale are a must to interpret geochronologic data from shear zones.

Based on combined $^{40}Ar/^{39}Ar$ muscovite, microstructural and oxygen isotopic data of the Columbia River Detachment (western Canada) and adjacent blocks, Mulch et al. (2006) inferred deformation migration and strain localization, since younger ages associated with decreasing deformation temperatures were progressively obtained towards the footwall. In the Dom Feliciano Belt (central Uruguay), regional metamorphism and cooling is recorded by K-Ar and $^{40}Ar/^{39}Ar$ mica ages of ca. 625-600 Ma in folded and thrusted metasedimentary rocks, which are crosscut by shear zones yielding ages of ca. 600-580 Ma (Oriolo et al., 2016b). This suggests that deformation at ca. 600-580 Ma was mostly localized into shear zones, thus contrasting with regional folding and thrusting at ca. 625-600 Ma (Oriolo et al., 2016b). In a similar way, coupled EMP Th-U-Pb monazite and thermobarometric data of the Central African Fold Belt (eastern Cameroon) allowed the recognition of low- and high-strain domains, recording high-temperature metamorphism and subsequent mylonitization, respectively (Tchato et al., 2009). Comparably, $^{40}Ar/^{39}Ar$ white mica ages of contrasting microstructural domains recording the timing of different HP metamorphic and mylonitic events were reported from the Western Alps by Villa et al. (2014).

7. Final remarks

The complexity that arises from the coupling between deformation, metamorphism and fluid-rock interaction prevents straightforward interpretation of geochronologic data of shear zones. In the first place, closure temperature calculations depend on cooling rate and grain size, but can also vary with pressure and mineral composition, among others. Deformation-related processes such as neocrystallization, recrystallization, fluid circulation and changes in deformation mechanisms may also play a major role in isotopic systems in shear zones. For this reason, thermochronologic data of mylonites have to be carefully evaluated in the light of detailed structural, microstructural and petrologic data and cannot be solely interpreted as a "cooling age" below closure temperature. In this context, structural data at different scales is critical. In addition to cooling, ages can record neo- or recrystallization, fluid-assisted deformation and/or inheritance from the protolith age. Hence, the concept of "closure temperature" has to be used with caution in shear zones.

Due to the ambiguity that may arise from isolated data, an integrated multiproxy approach is suggested to robustly assess the long-term evolution of crustal-scale shear zones. Thermochronologic data of mylonitic belts need to be combined with geochronologic data of associated intrusions and adjacent blocks, whereas structural and microstructural analysis is a must. For a certain structural domain, a multithermochronometric approach may be particularly useful, combining ages based on different thermochronometric systems. As a result, the integration of all these data allows reconstructing detailed P-T-ε-t paths of shear zones and neighboring areas, providing irreplaceable constraints on the tectonothermal evolution of the entire crust.

Future lines of investigation should quantitatively evaluate so far poorly explored aspects of isotopic diffusion, based on natural, theoretical and experimental data. In this sense, contributions such as the one by Liang (2017), who provided pressure-corrected equations to quantify the role of pressure in the diffusion model of Dodson (1973), are particularly encouraged. When possible, closure temperatures should be calculated for each particular case, based on independent estimations of P-T conditions, cooling rate, and grain size, among others. In this sense, *in situ* analytical methods seem to be extremely powerful, since they allow for robust interpretation of geochronologic data in the light of metamorphic and deformation microstructures (e.g., Fig. 10), which can be complemented with textural, mineral chemistry and thermobarometric data. The combined effects of isotopic decay and diffusion should be also considered, as shown by Blackburn et al. (2011) for lower crustal xenoliths.

In the particular case of shear zones, it is fundamental to integrate structural, microstructural and thermochronologic data of different structural domains. This implies, for instance, an evaluation of marginal vs. central areas of a shear zone, thus allowing to quantify which parts of the shear zone where active when, and helping to address the long-standing question of whether shear zones thicken or thin with time. A similar approach needs to be applied in shear zone networks in order to evaluate the timing of shearing in different parts of the network. Studies dealing with these questions may shed light on the role of strain hardening/softening processes, with deep implications for the understanding of strain partitioning and localization processes. In addition, combined structural, microstructural and geochronologic data may provide insights into the timescales and strain rates of shear zones, as shown by Müller et al. (2000b) by Rb-Sr microsampling dating of strain fringes.

Acknowledgements

The authors wish to thank Carlo Doglioni for the editorial handling as well as Elena Druguet and an anonymous reviewer for their critical comments, which significantly contributed to improve the manuscript. Bernhard Schulz acknowledges the contributions by Joachim Krause, Helmholtz-Zentrum Dresden Rossendorf, Helmholtz Institute Freiberg for Resource Technology, and Sabine Gilbricht, TU Freiberg, to the development of EMP monazite dating and automated SEM applications. The Deutsche Forschungsgemeinschaft founded the EMP monazite dating through several grants to Bernhard Schulz.

References

Angiboust, S., Harlov, D., 2017. Ilmenite breakdown and rutile-titanite stability in metagranitoids: natural observations and experimental results. Am. Mineral. 102, 1696–1708.
Apted, M.J., Liou, J.G., 1983. Phase relations among greenschist, epidote-amphibolite, and amphibolite in a basaltic system. Am. J. Sci. 283A, 328–354.
Ayers, J.C., Loflin, M., Miller, C.F., Barton, M.D., Coath, C.D., 2006. In situ oxygen isotope analysis of monazite as a monitor of fluid infiltration during contact metamorphism: Birch Creek Pluton aureole, White Mountains, eastern California. Geology 34, 653–656.
Barbarin, B., 1999. A review of the relationships between granitoid types, their origins and their geodynamic environments. Lithos 46, 605–626.
Bense, F.A., Wemmer, K., Löbens, S., Siegesmund, S., 2014. Fault gouge analyses: K-Ar illite dating, clay mineralogy and tectonic significance – a study from the Sierras Pampeanas, Argentina. Int. J. Earth Sci. 103, 189–218.
Bense, F., Costa, C., Oriolo, S., Löbens, S., Dunkl, I., Wemmer, K., Siegesmund, S., 2017. Exhumation history and landscape evolution of the Sierra de San Luis (Sierras Pampeanas, Argentina) – new insights from low-temperature thermochronological data. Andean Geol. 44, 275–306.
Berger, A., Stünitz, H., 1996. Deformation mechanisms and reaction of hornblende: examples from the Bergell tonalite (Central Alps). Tectonophysics 257, 149–174.
Bhadra, S., Das, S., Bhattacharya, A., 2007. Shear zone-hosted migmatites (Eastern India): the role of dynamic melting in the generation of REE-depleted felsic melts, and implications for disequilibrium melting. J. Petrol. 48, 435–457.
Black, R., Liégeois, J.-P., 1993. Cratons, mobile belts, alkaline rocks and continental lithospheric mantle: the Pan-African testimony. J. Geol. Soc. 150, 89–98.
Blackburn, T., Bowring, S.A., Schoene, B., Mahan, K., Dudas, F., 2011. U-Pb thermochronology: creating a temporal record of lithosphere thermal evolution. Contrib. Mineral. Petrol. 162, 479–500.
Bokuvská, Z., Jeřábek, P., Morales, L.F.G., 2016. Major softening at brittle-ductile transition due to interplay between chemical and deformation processes: An insight from evolution of shear bands in the South Armorican Shear Zone. J. Geophys. Res. https://doi.org/10.1002/2015JB012319.
Bonamici, C.E., Kozdon, R., Ushikubo, T., Valley, J.W., 2014. Intragrain oxygen isotope zoning in titanite by SIMS: Cooling rates and fluid infiltration along the Carthage-Colton Mylonite Zone, Adirondack Mountains, NY, USA. J. Metamorph. Geol. 32, 71–92.
Bossi, J., Campal, N., 1992. Magmatismo y tectónica transcurrente durante el Paleozoico inferior del Uruguay. In: Gutiérrez, J., Saavedra, J., Rábano, I. (Eds.), Paleozoico Inferior de Ibero-América. Universidad de Extremadura, Alicante, pp. 343–356.
Bozkurt, E., Satir, M., Buğdaycioğlu, Ç., 2011. Surprisingly young Rb/Sr ages from the Simav extensional detachment fault zone, northern Menderes Massif, Turkey. J. Geodyn. 52, 406–431.
Brandon, M.T., 2007. Closure Program, v. 1.2. In: Yale University.
Brandon, M.T., Roden-Tice, M.K., Garver, J.I., 1998. Late Cenozoic exhumation of the Cascadia accretionary wedge in the Olympic Mountains, Northwest Washington State. Geol. Soc. Am. Bull 110, 985–1009.
Braun, J., van der Beek, P., Batt, G., 2006. Quantitative Thermochronology. Cambridge University Press, Cambridge.
Brown, M., Solar, G.S., 1998. Shear-zone systems and melts: feedback relations and self-organization in orogenic belts. J. Struct. Geol. 20, 211–227.
Budzyń, B., Harlov, D.E., Williams, M.L., Jercinovic, M.J., 2011. Experimental determination of stability relations between monazite, fluorapatite, allanite, and REE-epidote as a function of pressure, temperature, and fluid composition. Am. Mineral. 96, 1547–1567.
Budzyń, B., Konečný, P., Kozub-Budzyń, G., 2015. Stability of monazite and disturbance of the Th-U-Pb system under experimental conditions of 250-350 °C and 200-400 MPa. Ann. Soc. Geol. Poland 85, 405–424.
Budzyń, B., Harlov, D.E., Kozub-Budzyń, G., Majka, J., 2017. Experimental constraints on the relative stabilities of the two systems monacite-(Ce)–allanite-(Ce)–fluorapatite and xenotime-(Y)–(Y,HREE)-rich epidote–(Y,HREE)-rich fluorapatite, in high Ca and Na-Ca environments under P-T conditions of 200-1000 MPa and 450-750 °C. Mineral. Petrol. 111, 183–217.
Caddick, M.J., Konopásek, J., Thompson, A.B., 2010. Preservation of garnet growth zoning and the durationg of prograde metamorphism. J. Petrol. 51, 2327–2347.
Cao, S., Neubauer, F., 2016. Deep crustal expressions of exhumed strike-slip fault systems: Shear zone initiation on rheological boundaries. Earth-Sci. Rev. 162, 155–176.
Carrapa, B., 2010. Resolving tectonic problems by dating detrital minerals. Geology 38, 191–192.
Carreras, J., Druguet, E., 1994. Structural zonation as a result of inhomogeneous non-coaxial deformation and its control on syntectonic intrusions: an example from the Cap de Creus area, eastern-Pyrenees. J. Struct. Geol. 16, 1525–1534.
Carreras, J., 2001. Zooming on Northern Cap de Creus shear zones. J. Struct. Geol. 23, 1457–1486.
Carreras, J., Druguet, E., Griera, A., 2005. Shear zone-related folds. J. Struct. Geol. 27, 1229–1251.

Carreras, J., Czeck, D.M., Druguet, E., Hudleston, P.J., 2010. Structure and development of an anastomosing network of ductile shear zones. J. Struct. Geol. 32, 656–666.
Carreras, J., Cosgrove, J.W., Druguet, E., 2013. Strain partitioning in banded and/or anisotropic rocks: Implications for inferring tectonic regimes. J. Struct. Geol. 50, 7–21.
Carvalho, B.B., Sawyer, E.W., Janasi, V.A., 2016. Crustal reworking in a shear zone: transformation of metagranite to migmatite. J. Metamorph. Geol. 34, 237–264.
Cassata, W.S., Renne, P.R., Shuster, D.L., 2009. Argon diffusion in plagioclase and implications for thermochronometry: a case of study from the Bushveld Complex, South Africa. Geochim. Cosmochim. Acta 73, 6600–6612.
Chamberlain, K.R., Bowring, S.A., 2000. Apatite-feldspar U-Pb thermochronometer: A reliable, mid-range (~450°C), diffusion-controlled system. Chem. Geol. 172, 173–200.
Chan, Y.-C., Crespi, J.M., Hodges, K.V., 2000. Dating cleavage formation in slates and phyllites with the $^{40}Ar/^{39}Ar$ laser microprobe: an example from the western New England Appalachians, USA. Terra Nova 12, 264–271.
Cheng, H., Liu, X.C., Vervoort, J.D., Wilford, D., Cao, D.D., 2016. Micro-sampling Lu-Hf geochronology reveals episodic garnet growth and multiple high-P metamorphic events. J. Metamorph. Geol. 34, 363–377.
Cherniak, D.J., 1993. Lead diffusion in titanite and preliminary results on the effects of radiation damage on Pb transport. Chem. Geol. 110, 177–194.
Cherniak, D.J., 1995. Diffusion of lead in plagioclase and K-feldspar: an investigation using Rutherford Backscattering and Resonant Nuclear Reaction Analysis. Contrib. Mineral. Petrol. 120, 358–371.
Cherniak, D.J., 2000. Pb diffusion in rutile. Contrib. Mineral. Petrol. 139, 198–207.
Cherniak, D.J., Pyle, J.M., 2008. Th diffusion in monazite. Chem. Geol. 256, 52–61.
Cherniak, D.J., Watson, E.B., 2000. Pb diffusion in zircon. Chem. Geol. 172, 5–24.
Cherniak, D.J., Watson, E.B., Grove, M., Harrison, T.M., 2004. Pb diffusion in monazite: A combined RBS/SIMS study. Geochim. Cosmochim. Acta 68, 829–840.
Chew, D.M., Spikings, R.A., 2015. Geochronology and thermochronology using apatite: Time and temperature, lower crust to surface. Elements 11, 189–194.
Clauer, N., 2013. The K-Ar and $^{40}Ar/^{39}Ar$ methods revisited for dating fine-grained K-bearing clay minerals. Chem. Geol. 354, 163–185.
Clauer, N., Zwingmann, H., Liewig, N., Wendling, R., 2012. Comparative $^{40}Ar/^{39}Ar$ and K-Ar dating of illite-type clay minerals: A tentative explanation for age identities and differences. Earth-Sci. Rev. 115, 76–96.
Clerc, C., Jolivet, L., Ringenbach, J.-C., 2015. Ductile extensional shear zones in the lower crust of a passive margin. Earth Planet. Sci. Lett. 431, 1–7.
Cocherie, A., Be Mezeme, E., Legendre, O., Fanning, C.M., Faure, M., Rossi, P., 2005. Electron-microprobe dating as a tool for determining the closure of Th-U-Pb systems in migmatitic monazites. Am. Mineral. 90, 607–618.
Cosca, M.A., 2013. Structural fabrics (K-Ar/Ar-Ar). In: Rink, W.J., Thompson, J.W. (Eds.), Encyclopedia of scientific dating methods. Springer, Dordrecht. https://doi.org/10.1007/978-94-007-6304-3_124.
Cosca, M., Stunitz, H., Bourgeix, A.-L., Lee, J.P., 2011. $^{40}Ar^*$ loss in experimentally deformed muscovite and biotite with implications for $^{40}Ar/^{39}Ar$ geochronology of naturally deformed rocks. Geochim. Cosmochim. Acta 75, 7759–7778.
Crone, A.J., Omdahl, E.M., 1987. Directions in Paleoseismology. U. S. Geological Survey, New Mexico.
Dahl, P.S., 1996. The crystal-chemical basis for Ar retention in micas: inferences from interlayer partitioning and implications for geochronology. Contrib. Mineral. Petrol. 123, 22–39.
Dahl, P.S., 1997. A crystal-chemical basis for Pb retention and fission-track annealing systematics in U-bearing minerals, with implications for geochronology. Earth Planet. Sci. Lett. 150, 277–290.
Dahl, P.S., Terry, M.P., Jercinovic, M.J., Williams, M.L., Hamilton, M.A., Foland, K.A., Clement, S.M., Friberg, L.M., 2005. Electron probe (Ultrachron) micronometry of metamorphic monazite: unraveling the timing of polyphase thermotectonism in the easternmost Wyoming craton (Black Hills, South Dakota). Am. Mineral. 90, 1712–1728.
Davids, C., Wemmer, K., Zwingmann, H., Kohlmann, F., Jacobs, J., Bergh, S.G., 2013. K-Ar illite and apatite fission track constraints on brittle faulting and the evolution of the northern Norwegian passive margin. Tectonophysics 608, 196–211.
Deckart, K., Clark, A.H., Celso, A.A., Ricardo, V.R., Bertens, A.N., Mortensen, J.K., Fanning, M., 2005. Magmatic and hydrothermal chronology of the giant Río Blanco porphyry copper deposit, Central Chile: Implications of an integrated U-Pb and $^{40}Ar/^{39}Ar$ database. Econ. Geol. 100, 905–934.
Dempster, T.J., Martin, J.C., Shipton, Z.K., 2008. Zircon dissolution in a ductile shear zone, Monte Rosa granite gneiss, northern Italy. Mineral. Mag. 72, 971–986.
Di Vincenzo, G., Ghiribelli, B., Giorgetti, G., Palmeri, R., 2001. Evidence of a close link between petrology and isotope records: constraints from SEM, EMP, TEM and in situ ^{40}Ar-^{39}Ar laser analyses on multiple generations of white micas (Lanterman Range, Antarctica). Earth Planet. Sci. Lett. 192, 389–405.
Di Vincenzo, G., Rocchi, S., Rossetti, F., Storti, F., 2004. ^{40}Ar-^{39}Ar dating of pseudotachylytes: the effect of clast-hosted extraneous argon in Cenozoic fault-generated friction melts from the West Antarctic Rift System. Earth Planet. Sci. Lett. 223, 349–364.
Dodson, M.H., 1973. Closure temperature in cooling geochronological and petrological systems. Contrib. Mineral. Petrol. 40, 254–274.
Doglioni, C., Barba, S., Carminati, E., Riguzzi, F., 2014. Fault on-off versus coseismic fluids reaction. Geosci. Frontiers 5, 767–780.
Doublier, M.P., Potel, S., Wemmer, K., 2015. The tectono-metamorphic evolution of the very low-grade hangingwall constrains two-stage gneiss dome formation in the Montagne Noire (Southern France). J. Metamorph. Geol. 33, 71–89.
Druguet, E., 2001. Development of high thermal gradients by coeval transpression and magmatism during the Variscan orogeny: insights from the Cap de Creus (Eastern Pyrenees). Tectonophysics 332, 275–293.
Druguet, E., Passchier, C.W., Carreras, J., Victor, P., den Brok, S.W.J., 1997. Analysis of a complex high-strain zone at Cap de Creus, Spain. Tectonophysics 280, 31–45.
Druguet, E., Czeck, D.M., Alsop, G.I., Bons, P.D., 2013. Preface: Deformation localization. J. Struct. Geol. 50, 1–4.
Druguet, E., Carreras, J., Mezger, J.E., 2018. Discussion on "Middle Jurassic shear zones at Cap de Creus (eastern Pyrenees, Spain): a record of pre-drift extension of the Piemonte-Ligurian Ocean?" Journal of the Geological Society, London 174, 289-300. J. Geol. Soc. 175, 187–188. https://doi.org/10.1144/jgs2017-042.
Ducea, M.N., Ganguly, J., Rosenberg, E.J., Patchett, P.J., Cheng, W., Isachsen, C., 2003. Sm-Nd dating of spatially controlled domains of garnet single crystals: a new method of high-temperature thermochronology. Earth Planet. Sci. Lett. 213, 31–42.
Dunlap, W.J., 1997. Neocrystallization or cooling? $^{40}Ar/^{39}Ar$ ages of white micas from low-grade mylonites. Chem. Geol. 143, 181–203.
Eberlei, T., Habler, G., Wegner, W., Schuster, R., Körner, W., Thöni, M., Abart, R., 2015. Rb/Sr isotopic and compositional retentivity of muscovite during deformation. Lithos 227, 161–178.
Eggleton, R.A., Banfield, J.F., 1985. The alteration of granitic biotite to chlorite. Am. Mineral. 70, 902–910.
Fandrich, R., Gu, Y., Burrows, D., Moeller, K., 2007. Modern SEM-based mineral liberation analysis. Int. J. Miner. Process. 84, 310–320.
Farley, K.A., 2000. Helium diffusion from apatite: General behaviour as illustrated by Durango fluorapatite. J. Geophys. Res 105, 2903–2914.
Finger, F., Broska, I., Roberts, M.P., Schermaier, A., 1998. Replacement of primary monazite by apatite-allanite-epidote coronas in an amphibolite-facies granite gneiss from the eastern Alps. Am. Mineral. 83, 248–258.
Finger, F., Krenn, E., Schulz, B., Harlov, D.E., Schiller, D., 2016. Satellite monazites in polymetamorphic basement rocks of the Alps: their origin and petrological significance. Am. Mineral. 101, 1094–1103.
Fitz Gerald, J.D., Stünitz, H., 1993. Deformation of granitoids at low metamorphic grade. I: Reactions and grain size reduction. J. Struct. Geol. 221, 269–297.
Fitz-Díaz, E., van der Pluijm, B., 2013. Fold dating: A new Ar/Ar illite dating application to constrain the age of deformation in shallow crustal rocks. J. Struct. Geol. 54, 174–179.
Forster, M., Lister, G., 2009. Core-complex-related extension of the Aegean lithosphere initiated at the Eocene-Oligocene transition. J. Geophys. Res. 114, B02401.
Forster, M.A., Lister, G.S., Lennox, P.G., 2014. Dating deformation using crushed alkali feldspar: $^{40}Ar/^{39}Ar$ geochronology of shear zones in the Wyangala Batholith, NSW, Australia. Aust. J. Earth Sci. 61, 619–629.
Fossen, H., Cavalcante, G.C.G., 2017. Shear zones – A review. Earth-Sci. Rev. 171, 434–455.
Fossen, H., Dunlap, W.J., 1998. Timing and kinematics of Caledonian thrusting and extensional collapse, southern Norway: evidence from $^{40}Ar/^{39}Ar$ thermochronology. J. Struct. Geol. 20, 765–781.
Fossen, H., Tikoff, B., 1997. Forward modeling of non steady-state deformations and the minimum strain path. J. Struct. Geol. 19, 987–996.
Fossen, H., Tikoff, B., 1998. Extended models of transpression and transtension, and application to tectonic settings. In: Dewey, J.F., Holdsworth, R.E., Strachan, R.A. (Eds.), Continental Transpressional and Transtensional Tectonics. vol. 135. Geological Society of London Special Publications, London, pp. 15–33.
Fossen, H., Khani, H.F., Faleide, J.I., Ksienzyk, A.K., Dunlap, W.J., 2016. Post-Caledonian extension in the West Norway-northern North Sea region: the role of structural inheritance. In: Childs, C., Holdsworth, R.E., Jackson, C.A.-L., Manzocchi, T., Walsh, J.J., Yielding, G. (Eds.), The Geometry and Growth of Normal Faults. vol. 439. Geological Society of London Special Publications, London, pp. 465–486.
Freeman, S.R., Inger, S., Butler, R.W.H., Cliff, R.A., 1997. Dating deformation using Rb-Sr in white mica: Greenschist facies deformation from the Entrelor shear zone, Italian Alps. Tectonics 16, 57–76.
Frey, M., 1987. Very low-grade metamorphism of clastic sedimentary rocks. In: Frey, M. (Ed.), Low Temperature Metamorphism. Blackie, London.
Frost, B.R., Chamberlain, K.R., Schumacher, J.C., 2000. Sphene (titanite): Phase relations and role as a geochronometer. Chem. Geol. 172, 131–148.
Ganguly, J., Tirone, M., 1999. Diffusion closure temperature and age of a mineral with arbitrary extent of diffusion: theoretical formulation and applications. Earth Planet. Sci. Lett. 170, 131–140.
Ganguly, J., Ito, M., Zhang, X., 2007. Cr diffusion in orthopyroxene: Experimental determination, ^{53}Mn-^{53}Cr thermochronology, and planetary applications. Geochim. Cosmochim. Acta 71, 3915–3925.
García-Ruiz, S., Moldovan, M., García Alonso, J.I., 2008. Measurement of strontium isotope ratios by MC-ICP-MS after on-line Rb-Sr ion chromatography separation. J. Anal. At. Spectrom. 23, 84–93.
Gasser, D., Jeřábek, P., Faber, C., Stünitz, H., Menegon, L., Corfu, F., Erambert, M., Whitehouse, M.J., 2015. Behaviour of geochronometers and timing of metamorphic reactions during deformation at lower crustal conditions: phase equilibrium modelling and U-Pb dating of zircon, monazite, rutile and titanite from the Kalak Nappe Complex, northern Norway. J. Metamorph. Geol. 33, 513–534. https://doi.org/10.1111/jmg.12131.
Geisler, T., Schaltegger, U., Tomaschek, F., 2017. Re-equilibration of zircon in aqueous fluids and melts. Elements 3, 43–50.
Giletti, B.J., 1974. Studies in diffusion I: argon in phlogopite mica. In: Hofmann, A.W., Giletti, B.J., Yoder Jr.H.S., Yund, R.A. (Eds.), Geochemical Transport and Kinetics. vol. 634. Carnegie Institution of Washington, Washington, pp. 107–116.
Giletti, B.J., Yund, R.A., 1984. Oxygen diffusion in quartz. J. Geophys. Res. 89, 4039–4046.
Goncalves, P., Oliot, E., Marquer, D., Connolly, J.A.D., 2012. Role of chemical processes on shear zone formation: an example from the Grimsel metagranodiorite (Aar massif,

Central Alps). J. Metamorph. Geol. 30, 703–722.
Grégoire, V., Nédélec, A., Monié, P., Montel, J.-M., Ganne, J., Ralison, B., 2009. Structural reworking and heat transfer related to the late-Panafrican Angavo shear zone of Madagascar. Tectonophysics 477, 197–216.
Grove, M., Harrison, T.M., 1996. ^{40}Ar* diffusion in Fe-rich biotite. Am. Mineral. 81, 940–951.
Gueydan, F., Leroy, Y.M., Jolivet, L., 2004. Mechanics of low-angle extensional shear zones at the brittle-ductile transition. J. Geophys. Res. 109, B12407.
Halls, H.C., Campal, N., Davis, D.W., Bossi, J., 2001. Magnetic studies and U-Pb geochronology of the Uruguayan dike swarm, Rio de la Plata Craton, Uruguay: paleomagnetic and economic implications. J. S. Am. Earth Sci. 14, 349–361.
Hames, W.E., Bowring, S.A., 1994. An empirical evaluation of the Ar diffusion geometry in muscovite. Earth Planet. Sci. Lett. 124, 161–167.
Harbi, H.M., Ali, K.A., McNaughton, N.J., Andresen, A., 2017. U-Pb zircon and ^{40}Ar/^{39}Ar geochronology of sericite from hydrothermal alteration zones: new constraints for the timing of Ediacaran gold mineralization in the Sukhaybarat area, western Afif terrane, Saudi Arabia. Miner. Deposita. https://doi.org/10.1007/s00126-017-0751-7.
Harley, S.L., Kelly, N.M., Möller, A., 2007. Zircon behaviour and the thermal histories of mountain chains. Elements 3, 25–30.
Harlov, D., 2015. Fluids and geochronometers: Charting and dating mass transfer during metasomatism and metamorphism. J. Indian I. Sci. 95, 109–123.
Harlov, D.E., Wirth, R., Hetherington, C.J., 2011. Fluid-mediated partial alteration of monazite: the role of coupled dissolution-reprecipitation during apparent solid state element mass transfer. Contrib. Mineral. Petrol. 162, 329–348.
Harrison, T.M., 1981. Diffusion of ^{40}Ar in hornblende. Contrib. Mineral. Petrol. 78, 324–331.
Harrison, T.M., Zeitler, P.K., 2005. Fundamentals of noble gas thermochronometry. Rev. Mineral. Geochem. 58, 123–149.
Harrison, T.M., Duncan, I., McDougall, I., 1985. Diffusion of ^{40}Ar in biotite – temperature, pressure and compositional effects. Geochim. Cosmochim. Acta 49, 2461–2468.
Harrison, T.M., Célérier, J., Aikman, A.B., Hermann, J., Heizler, M.T., 2009. Diffusion of ^{40}Ar in muscovite. Geochim. Cosmochim. Acta 73, 1039–1051.
Haselton Jr., H.T., Cygan, G.L., Jenkins, D.M., 1995. Experimental study of muscovite stability in pure H_2O and 1 molal KCl-HCl solutions. Geochim. Cosmochim. Acta 59, 429–442.
Hnat, J.S., van der Pluijm, B.A., 2014. Fault gouge dating in the Southern Appalachians, USA. Geol. Soc. Am. Bull. 126, 639–651.
Hobbs, B.E., Mülhaus, H.B., Ord, A., 1990. Instability, softening and localization of deformation. In: Knipe, R.J., Rutter, E.H. (Eds.), Deformation mechanisms, Rheology and Tectonics. 55. Geological Society of London Special Publications, London, pp. 143–165.
Hogmalm, K.J., Zack, T., Karlsson, A.K.-O., Sjöqvist, A.S.L., Garbe-Schönberg, D., 2017. In situ Rb-Sr and K-Ca dating by LA-ICP-MS/MS: an evaluation of N_2O and SF_6 reaction gases. J. Anal. At. Spectrom. 32, 305–313.
Hueck, M., Oriolo, S., Dunkl, I., Wemmer, K., Oyhantçabal, P., Schanofski, M., Basei, M.A.S., Siegesmund, S., 2017. Phanerozoic low-temperature evolution of the Uruguayan Shield along the South American passive margin. J. Geol. Soc. 174, 609–626.
Hunziker, J.C., Frey, M., Clauer, N., Dallmeyer, R.D., Friedrichsen, H., Flehmig, W., Hochstrasser, K., Roggwiler, P., Schwander, H., 1986. The evolution of illite to muscovite: mineralogical and isotopic data from the Glarus Alps, Switzerland. Contrib. Mineral. Petrol. 92, 157–180.
Hutton, D.H.W., Dempster, T.J., Brown, P.E., Becker, S.D., 1990. A new mechanism of granite emplacement: intrusion in active extensional shear zones. Nature 343, 452–455.
Jäger, E., 1977. Introduction to geochronology. In: Jäger, E., Hunziker, J. (Eds.), Lectures of Isotope Geology. Springer, Heidelberg, pp. 1–12.
Jäger, E., Niggli, E., Wenk, E., 1967. Rb-Sr Altersbestimmungen an Glimmern der Zentralalpen. In: Beiträge zur Geologischen Karte der Schweiz. vol. 134 Kümmerly & Frey, Bern.
Janots, E., Brunet, F., Goffé, B., Poinssot, C., Burchard, M., Cemic, L., 2007. Thermochemistry of monazite-(La) and dissakisite-(La): implications for monazite and allanite stability in metapelites. Contrib. Mineral. Petrol. 154, 1–14.
Jefferies, S.P., Holdsworth, R.E., Wibberley, C.A.J., Shimamoto, T., Spiers, C.J., Niemeijer, A.R., Lloyd, G.E., 2006. The nature and importance of phyllonite development in crustal-scale fault cores: an example form the Median Tectonic Line, Japan. J. Struct. Geol. 28, 220–235.
Jenkin, G.R.T., 1997. Mode effects on cooling rate estimates from Rb-Sr data. Geology 25, 907–910.
Jenkin, G.R.T., Ellam, R.M., Rogers, G., Stuart, F.M., 2001. An investigation of closure temperature of the biotite Rb-Sr system: The importance of cation exchange. Geochim. Cosmochim. Acta 65, 1141–1160.
Jercinovic, M.J., Williams, M.L., Lane, E.D., 2008. In-situ trace element analysis of monazite and other fine-grained accessory minerals by EMPA. Chem. Geol. 254, 197–215.
Johnson, S.E., 1999. Porphyroblast microstructures; a review of current and future trends. Am. Mineral. 84, 1711–1726.
Jones, R.R., Tanner, P.W.G., 1995. Strain partitioning in transpression zones. J. Struct. Geol. 17, 793–802.
Just, J., Schulz, B., de Wall, H., Jourdan, F., Pandit, M.K., 2010. Monazite CHIME/EPMA dating of Erinpura granitoid deformation: implications for Neoproterozoic tectonothermal evolution of NW India. Gondwana Res. 19, 402–412.
Kapp, P., Manning, E., Tropper, P., 2009. Phase-equilibrium constraints on titanite and rutile activities in mafic epidote amphibolites and geobarometry using titanite-rutile equilibria. J. Metamorph. Geol. 27, 509–521.
Kelley, S., 2002. K-Ar and Ar-Ar Dating. Rev. Mineral. Geochem. 47, 785–818. https://doi.org/10.2138/rmg.2002.47.17.
Kirschner, D.L., Teyssier, C., Gregory, R.T., Sharp, Z.D., 1995. Effect of deformation on oxygen isotope exchange in the Heavitree Quartzite, Ruby Gap duplex, central Australia. J. Struct. Geol. 17, 1407–1423.
Kirschner, D.L., Cosca, M.A., Masson, H., Hunziker, J.C., 1996. Staircase ^{40}Ar/^{39}Ar spectra of fine-grained white mica: Timing and duration of deformation and empirical constraints on argon diffusion. Geology 24, 747–750.
Kisch, H.J., 1987. Correlation between indicators of very low-grade metamorphism. In: Frey, M. (Ed.), Low Temperature Metamorphism. Blackie, London.
Kolb, J., 2008. The role of fluids in partitioning brittle deformation and ductile creep in auriferous shear zones between 500 and 700 °C. Tectonophysics 446, 1–15.
Kooijman, E., Mezger, K., Berndt, J., 2010. Constraints on the U-Pb systematics of metamorphic rutile from in situ LA-ICP-MS analysis. Earth Planet. Sci. Lett. 293, 321–330.
Kovaleva, E., Klötzli, U., Wheeler, J., Habler, G., 2018. Mechanisms of strain accomodation in plastically-deformed zircon under simple shear deformation conditions during amphibolite-facies metamorphism. J. Struct. Geol. 107, 12–24.
Krenn, E., Schulz, B., Finger, F., 2012. Three generations of monazite in Austroalpine basement rocks to the south of the Tauern Window – evidences for Variscan, Permian and Alpine metamorphism. Swiss J. Geosci. 105, 1–18.
Kröner, A., Wan, Y., Liu, X., Liu, D., 2014. Dating of zircon from high-grade rocks: Which is the most reliable method? Geosci. Frontiers 5, 515–523.
Kruhl, J.H., 1996. Prism- and basal-plane parallel subgrain boundaries in quartz: a microstructural geothermobarometer. J. Metamorph. Geol. 14, 581–589.
Ksienzyk, A.K., Wemmer, K., Jacobs, J., Fossen, H., Schomberg, A.C., Süssenberger, A., Lünsdorf, N.K., Bastesen, E., 2016. Post-Caledonian brittle deformation in the Bergen area, West Norway: results from K-Ar illite fault gouge dating. Norwegian J. Geol. 96, 275–299.
Kübler, B., 1964. Les argiles, indicateurs de métamorphisme. Rev. Inst. Franç. Pétrol. 19, 1093–1112.
Law, R.D., 2014. Deformation thermometry based on quartz c-axis fabrics and recrystallization microstructures: A review. J. Struct. Geol. 66, 129–161.
Le Bas, M.J., Le Maitre, R.W., Streckeisen, A., Zanettin, B., 1986. A chemical classification of volcanic rocks based on the Total Alkali-Silica diagram. J. Petrol. 27, 745–750.
Lee, J.K.W., Williams, I.S., Ellis, D.J., 1997. Pb, U and Th diffusion in natural zircon. Nature 390, 159–162.
Liang, Y., 2017. Effect of pressure on closure temperature of a trace element in cooling petrological systems. Contrib. Mineral. Petrol. https://doi.org/10.1007/s00410-016-1327-8.
Liégeois, J.-P., Abdesalam, M.G., Ennih, N., Ouabadi, A., 2013. Metacraton: nature, genesis and behavior. Gondwana Res. 23, 220–237.
Lisle, R.J., 2014. Strain analysis in dilatational shear zones, with examples from Marloes, SW Wales. In: Llana-Fúnez, S., Marcos, A., Bastida, F. (Eds.), Deformation Structures and Processes Within the Continental Crust. 394. Geological Society of London Special Publications, London, pp. 7–20.
Lister, G.S., Baldwin, S.L., 1996. Modelling the effect of arbitrary P-T-t histories on Ar diffusion in minerals using the MacArgon program for the Apple Macintosh. Tectonophysics 253, 83–109.
Lister, G.S., Williams, P.F., 1983. The partitioning of deformation in flowing rock masses. Tectonophysics 92, 1–33.
Löbens, S., Bense, F.A., Wemmer, K., Dunkl, I., Costa, C.H., Layer, P., Siegesmund, S., 2011. Exhumation and uplift of the Sierras Pampeanas: preliminary implications from K-Ar fault gouge dating and low-T thermochronology in the Sierra de Comechingones (Argentina). Int. J. Earth Sci. 100, 671–694.
Löbens, S., Oriolo, S., Benowitz, J., Wemmer, K., Layer, P., Siegesmund, S., 2017. Late Paleozoic deformation and exhumation in the Sierras Pampeanas (Argentina): ^{40}Ar/^{39}Ar-feldspar dating constraints. Int. J. Earth Sci. 106, 1991–2003.
Lovera, O.M., Richter, F.M., Harrison, T.M., 1989. The ^{40}Ar/^{39}Ar thermochronometry for slowly cooled samples having a distribution of diffusion domain sizes. J. Geophys. Res. 94, 17917–17935.
MacDonald, J.M., Wheeler, J., Harley, S.L., Mariani, E., Goodenough, K.M., Crowley, Q., Tatham, D., 2013. Lattice distortion in a zircon population and its effects on trace element mobility and U-Th-Pb isotope systematics: examples from the Lewisian Gneiss Complex, northwest Scotland. Contrib. Mineral. Petrol. 166, 21–41.
Maffini, M.N., Wemmer, K., Radice, S., Oriolo, S., D'Eramo, F., Coniglio, J., Demartis, M., Pinotti, L., 2017. Polymetallic (Pb-Zn-Cu-Ag ± Au) vein-type deposits in brittle-ductile transtensional shear zones, Eastern Sierras Pampeanas (Argentina): Age constraints and significance for the Late Paleozoic tectonic evolution and metallogenesis. Ore Geol. Rev. 89, 668–682.
Mancktelow, N.S., 2006. How ductile are ductile shear zones? Geology 34, 345–348.
Marsh, J.H., Johnson, S.E., Yates, M.G., West Jr., D.P., 2009. Coupling of deformation and reactions during mid-crustal shear zone development: an *in situ* frictional-viscous transition. J. Metamorph. Geol. 27, 531–553. https://doi.org/10.1111/j.1525-1314.2009.00841.x.
McDougall, I., Harrison, T.M., 1999. Geochronology and Thermochronology by the ^{40}Ar/^{39}Ar method. Oxford University Press, New York.
McFarlane, C.R.M., Harrison, T.M., 2006. Pb-difussion in monazite: Constraints from a high-T contact aureole setting. Earth Planet. Sci. Lett. 250, 376–384.
McWilliams, C.K., Wintsch, R.P., Kunk, M.J., 2007. Scales of equilibrium and disequilibrium during cleavage formation in chlorite and biotite-grade phyllites, SE Vermont. J. Metamorph. Geol. 25, 895–913.
Mezger, K., Krogstad, E.J., 1997. Interpretation of discordant U-Pb zircon ages: An evaluation. J. Metamorph. Geol. 15, 127–140.
Mezger, K., Essene, E.J., Halliday, A.N., 1992a. Closure temperatures of the Sm-Nd system in metamorphic garnets. Earth Planet. Sci. Lett. 193, 397–409.
Mezger, K., van der Pluijm, B.A., Essene, E.J., Halliday, A.N., 1992b. The Carthage-Colton

Mylonite Zone (Adirondack Mountains, New York): The site of a cryptic suture in the Grenville Orogen? J. Geol. 100, 630–638.
Micklethwaite, S., Sheldon, H.A., Baker, T., 2010. Active fault and shear processes and their implications for mineral deposit formation and discovery. J. Struct. Geol. 32, 151–165.
Mittempergher, S., Dallai, L., Pennacchioni, G., Renard, F., Di Toro, G., 2014. Origin of hydrous fluids at seismogenic depth: Constraints from natural and experimental fault rocks. Earth Planet. Sci. Lett. 385, 97–109.
Montel, J.M., Foret, S., Veschambre, M., Nicollet, Ch., Provost, A., 1996. Electron microprobe dating of monazite. Chem. Geol. 131, 37–53.
Montési, L.G.J., 2013. Fabric development as the key for forming ductile shear zones and enabling plate tectonics. J. Struct. Geol. 50, 254–266.
Mulch, A., Cosca, M.A., 2004. Recrystallization or cooling ages: in situ UV-laser $^{40}Ar/^{39}Ar$ geochronology of muscovite in mylonitic rocks. J. Geol. Soc. 161, 573–582.
Mulch, A., Cosca, M.A., Handy, M.R., 2002. In-situ UV-laser $^{40}Ar/^{39}Ar$ geochronology of a micaceous mylonite: an example of defect-enhanced argon loss. Contrib. Mineral. Petrol. 142, 738–752.
Mulch, A., Teyssier, C., Cosca, M.A., Vennemann, T.W., 2006. Thermomechanical analysis of strain localization in a ductile detachment zone. J. Geophys. Res. 111, B12405.
Müller, W., Mancktelow, N.S., Meier, M., 2000a. Rb-Sr microchrons of synkinematic mica in mylonites: an example from the DAV fault of the Eastern Alps. Earth Planet. Sci. Lett. 180, 385–397.
Müller, W., Aerden, D., Halliday, A.N., 2000b. Isotopic dating of strain fringe increments: duration and rates of deformation in shear zones. Science 288, 2195–2198.
O'Hara, K., Blackburn, W.H., 1989. Volume-loss model for trace-element enrichments in mylonites. Geology 17, 524–527.
O'Hara, K.D., Sharp, Z.D., Moecher, D.P., Jenkin, G.R.T., 1997. The effect of deformation on oxygen exchange in quartz and feldspar and the significance of isotopic temperatures in mylonites. J. Geol. 105, 193–204.
Oriolo, S., Oyhantçabal, P., Heidelbach, F., Wemmer, K., Siegesmund, S., 2015. Structural evolution of the Sarandí del Yí Shear Zone: kinematics, deformation conditions and tectonic significance. Int. J. Earth Sci. 104, 1759–1777.
Oriolo, S., Oyhantçabal, P., Wemmer, K., Basei, M.A.S., Benowitz, J., Pfänder, J., Hannich, F., Siegesmund, S., 2016a. Timing of deformation in the Sarandí del Yí Shear Zone, Uruguay: implications for the amalgamation of Western Gondwana during the Neoproterozoic Brasiliano–Pan-African Orogeny. Tectonics 35, 754–771.
Oriolo, S., Oyhantçabal, P., Wemmer, K., Heidelbach, F., Pfänder, J., Basei, M.A.S., Hueck, M., Hannich, F., Sperner, B., Siegesmund, S., 2016b. Shear zone evolution and timing of deformation in the Neoproterozoic transpressional Dom Feliciano Belt, Uruguay. J. Struct. Geol. 92, 59–78.
Oriolo, S., Oyhantçabal, P., Basei, M.A.S., Wemmer, K., Siegesmund, S., 2016c. The Nico Pérez Terrane (Uruguay): From Archean crustal growth and connections with the Congo Craton to late Neoproterozoic accretion to the Río de la Plata Craton. Precambrian Res. 280, 147–160.
Oriolo, S., Hueck, M., Oyhantçabal, P., Goscombe, B., Wemmer, K., Siegesmund, S., 2018. Shear zones in Brasiliano–Pan-African belts and their role in the amalgamation and break-up of southwestern Gondwana. In: Siegesmund, S., Basei, M.A.S., Oyhantçabal, P., Oriolo, S. (Eds.), Geology of Southwest Gondwana. Springer International Publishing, pp. 593–613.
Oyhantçabal, P., Muzio, R., de Souza, S., 1993. Geología y aspectos estructurales del borde orogénico en el extremo sur del cinturón Dom Feliciano. Rev. Bras. Geociências 23, 296–300.
Oyhantçabal, P., Heimann, A., Miranda, S., 2001. Measurement and interpretation of strain in the syntectonic Solís de Mataojo Granitic Complex, Uruguay. J. Struct. Geol. 23, 807–817.
Oyhantçabal, P., Siegesmund, S., Wemmer, K., Frei, R., Layer, P., 2007. Post-collisional transition from calc-alkaline to alkaline magmatism during transcurrent deformation in the southernmost Dom Feliciano Belt (Braziliano–Pan-African, Uruguay). Lithos 98, 141–159.
Oyhantçabal, P., Siegesmund, S., Wemmer, K., Layer, P., 2010. The Sierra Ballena Shear Zone in the southernmost Dom Feliciano Belt (Uruguay): evolution, kinematics, and deformation conditions. Int. J. Earth Sci. 99, 1227–1246.
Oyhantçabal, P., Siegesmund, S., Wemmer, K., Presnyakov, S., Layer, P., 2009b. Geochronological constraints on the evolution of the southern Dom Feliciano Belt (Uruguay). J. Geol. Soc. 166, 1075–1084.
Oyhantçabal, P., Siegesmund, S., Wemmer, K., Passchier, C.W., 2011a. The transpressional connection between Dom Feliciano and Kaoko Belts at 580-550 Ma. Int. J. Earth Sci. 100, 379–390.
Oyhantçabal, P., Siegesmund, S., Wemmer, K., 2011b. The Río de la Plata Craton: a review of units, boundaries, ages and isotopic signature. Int. J. Earth Sci. 100, 201–220.
Oyhantçabal, P., Wegner-Eimer, M., Wemmer, K., Schulz, B., Frei, R., Siegesmund, S., 2012. Paleo- and Neoproterozoic magmatic and tectonometamorphic evolution of the Isla Cristalina de Rivera (Nico Pérez Terrane, Uruguay). Int. J. Earth Sci. 101, 1745–1762.
Oyhantçabal, P., Oriolo, S., Philipp, R.P., Wemmer, K., Siegesmund, S., 2018. The Nico Pérez Terrane of Uruguay and southeastern Brazil. In: Siegesmund, S., Basei, M.A.S., Oyhantçabal, P., Oriolo, S. (Eds.), Geology of Southwest Gondwana. Springer International Publishing, pp. 161–188.
Parry, W.T., Downey, L.M., 1982. Geochemistry of hydrothermal chlorite replacing igneous biotite. Clay. Clay Miner. 30, 81–90.
Parry, W.T., Bunds, M.P., Bruhn, R.L., Hall, C.M., Murphy, J.M., 2001. Mineralogy, $^{40}Ar/^{39}Ar$ dating and apatite fission track dating of rocks along the Castle Mountain fault, Alaska. Tectonophysics 337, 149–172.
Passchier, C.W., Platt, J.P., 2017. Shear zone junctions: Of zippers and freeways. J. Struct. Geol. 95, 188–202.
Paterson, S.R., Vernon, R.H., Tobisch, O.T., 1989. A review of criteria for the identification of magmatic and tectonic foliations in granitoids. J. Struct. Geol. 11, 349–363.
Paterson, S.R., Fowler Jr., T.K., Schmidt, K.L., Yoshinobu, A.S., Yuan, E.S., Miller, R.B., 1998. Interpreting magmatic fabric patterns in plutons. Lithos 44, 53–82.
Platt, J.P., Behr, W.M., 2011a. Grainsize evolution in ductile shear zones: Implications for strain localization and the strength of the lithosphere. J. Struct. Geol. 33, 537–550.
Platt, J.P., Behr, W.M., 2011b. Lithospheric shear zones as constant stress experiments. Geology 39, 127–130.
Pollington, A.D., Baxter, E.F., 2011. High precision microsampling and preparation of zoned garnet porphyroblasts for Sm-Nd geochronology. Chem. Geol. 281, 270–282.
Précigout, J., Prigent, C., Palasse, L., Pochon, A., 2017. Water pumping in mantle shear zones. Nat. Commun. 8, 15736.
Pryer, L.L., 1993. Microstructures in feldspars from a major crustal thrust zone: the Grenville Front, Ontario. Canada. J. Struct. Geol. 15, 21–36.
Purdy, J.W., Jäger, E., 1976. K-Ar ages on rock-forming minerals from the Central Alps. Mem. Inst. Geol. Mineral. Univ. Padova 30, 1–31.
Pyle, J.M., Spear, F.S., Wark, D.A., Daniel, C.G., Storm, L.C., 2005. Contribution to precision and accuracy of monazite microprobe ages. Am. Mineral. 90, 547–577.
Ramsay, J.G., 1980. Shear zone geometry: a review. J. Struct. Geol. 2, 83–99.
Reddy, S.M., Timms, N.E., Trimby, P., Kinny, P.D., Buchan, C., Blake, K., 2006. Crystal-plastic deformation of zircon: A defect in the assumption of chemical robustness. Geology 34, 257–260.
Reich, M., Ewing, R.C., Ehlers, T.A., Becker, U., 2007. Low-temperature anisotropic diffusion of helium in zircon: Implications for zircon (U-Th)/He thermochronometry. Geochim. Cosmochim. Acta 71, 3119–3130.
Reiners, P.W., Brandon, M.T., 2006. Using thermochronology to understand orogenic erosion. Annu. Rev. Earth Planet. Sci. 34, 419–466.
Reiners, P.W., Ehlers, T.A., Zeitler, P.K., 2005. Past, present, and future of thermochronology. Rev. Mineral. Geochem. 58, 1–18.
Ring, U., Uysal, I.T., Glodny, J., Cox, S.C., Little, T., Thomson, S.N., Stübner, K., Bozkaya, Ö., 2017. Fault-gouge dating in the Southern Alps, New Zealand. Tectonophysics 717, 321–338.
Robbins, G.A., 1972. Radiogenic Ar Diffusion in Muscovite under Hydrothermal Conditions. M.Sc Thesis. Brown University.
Rosenberg, C.L., 2004. Shear zones and magma ascent: A model based on a review of the Tertiary magmatism in the Alps. Tectonics 23, TC3002.
Sambridge, M.S., Compston, W., 1994. Mixture modelling of multicomponent data sets with application to ion-probe zircons. Earth Planet. Sci. Lett. 128, 373–390.
Santos, J.O.S., Hartmann, L.A., Bossi, J., Campal, N., Schipilov, A., Piñeyro, D., McNaughton, N.J., 2003. Duration of the Trans-Amazonian cycle and its correlation within South America based on U-Pb SHRIMP Geochronology of the La Plata Craton, Uruguay. Int. Geol. Rev. 45, 27–48.
Sassier, C., Leloup, P.H., Rubatto, D., Galland, D., Galland, O., Yue, Y., Lin, D., 2009. Direct measurement of strain rates in ductile shear zones: A new method based on syntectonic dikes. J. Geophys. Res. 114, B01406.
Schaltegger, U., Schmitt, A.K., Horstwood, M.S.A., 2015. U-Th-Pb zircon geochronology by ID-TIMS, SIMS, and laser ablation ICP-MS: Recipes, interpretations, and opportunities. Chem. Geol. 402, 89–110.
Schneider, S., Hammerschmidt, K., Rosenberg, C.L., 2013. Dating the longevity of shear zones: Insight from $^{40}Ar/^{39}Ar$ in situ analysis. Earth Planet. Sci. Lett. 369-370, 43–58.
Schoene, B., 2014. U-Th-Pb geochronology, in: Rudnick, R.L. (Ed.), treatise on Geochemistry, the crust. Elsevier, Amsterdam 4, 341–378. https://doi.org/10.1016/B978-0-08-095975-7.00310-7.
Schoene, B., Bowring, S.A., 2007. Determining accurate temperature-time paths from U-Pb thermochronology: An example from the Kaapvaal craton, southern Africa. Geochim. Cosmochim. Acta 71, 165–185.
Schulz, B., 2017. Polymetamorphism in garnet micaschists of the Saualpe Eclogite Unit (Eastern Alps, Austria), resolved by automated SEM methods and EMP-Th-U-Pb monazite dating. J. Metamorph. Geol. 35, 141–163.
Schulz, B., Schüssler, U., 2013. Electron-microprobe Th-U-Pb monazite dating in Early-Palaeozoic high-grade gneisses as a completion of U-Pb isotopic ages (Wilson Terrane, Antarctica). Lithos 175-176, 178–192.
Schulz, B., von Raumer, J.F., 2011. Discovery of Ordovician-Silurian metamorphic monazite in garnet metapelites of the Alpine External Aiguilles Rouges Massif. Swiss J. Geosci. 104, 67–79.
Shaw, C.A., Karlstrom, K.E., Williams, M.L., Jercinovic, M.J., McCoy, A.M., 2001. Electron-microprobe monazite dating of ca. 1.71-1.63 Ga and ca. 1.45-1.38 Ga deformation in the Homestake shear zone, Colorado: Origin and early evolution of a persistent intracontinental tectonic zone. Geology 29, 739–742.
Sherlock, S.C., Hetzel, R., 2001. A laser-probe $^{40}Ar/^{39}Ar$ study of pseudotachylite from the Tambach Fault Zone, Kenya: direct isotopic dating of brittle faults. J. Struct. Geol. 23, 33–44.
Sherlock, S.C., Kelley, S.P., Zalasiewicz, J.A., Schofield, D.I., Evans, J.A., Merriman, R.J., Kemp, S.J., 2003. Precise dating of low-temperature deformation: Strain-fringe analysis by ^{40}Ar-^{39}Ar laser microprobe. Geology 31, 219–222.
Sibson, R.H., 1977. Fault rocks and fault mechanisms. J. Geol. Soc. 133, 191–213.
Sibson, R.H., 1983. Continental fault structure and the shallow earthquake source. J. Geol. Soc. 140, 741–767.
Sibson, R.H., 1990. Conditions for fault-valve behaviour. In: Knipe, R.J., Rutter, E.H. (Eds.), Deformation Mechanisms, Rheology and Tectonics. 54. Geological Society of London Special Publications, London, pp. 15–28.
Siegesmund, S., Steenken, A., López de Luchi, M.G., Wemmer, K., Hoffmann, A., Mosch, S., 2004. The Las Chacras-Potrerillos batholith (Pampean Ranges, Argentina): structural evidences, emplacement and timing of the intrusion. Int. J. Earth Sci. 93, 23–43.
Siegesmund, S., Layer, P., Dunkl, I., Vollbrecht, A., Steenken, A., Wemmer, K., Ahrendt, H., 2008. Exhumation and deformation history of the lower crustal section of the

Valstrona di Omegna in the Ivrea Zone, southern Alps. In: Siegesmund, S., Fügenschuh, B., Froitzheim, N. (Eds.), Tectonic Aspects of the Alpine-Dinaride-Carpathian System. 298. Geological Society of London Special Publications, London, pp. 45–68.
Simpson, C., 1986. Fabric development in brittle-to-ductile shear zones. Pure Appl. Geophys. 124, 269–288.
Skrzypek, E., Schulmann, K., Štípská, P., Chopin, F., Lehmann, J., Lexa, O., Haloda, J., 2011. Tectono-metamorphic history recorded in garnet porphyroblasts: insights from thermodynamic modelling and electron backscatter diffraction analysis of inclusion trails. J. Metamorph. Geol. 29, 473–496.
Smeraglia, L., Berra, F., Billi, A., Boschi, C., Carminati, E., Doglioni, C., 2016. Origin and role of fluids involved in the seismic cycle of extensional faults in carbonate rocks. Earth Planet. Sci. Lett. 450, 292–305.
Smit, M.A., Scherer, E.E., Mezger, K., 2013. Lu-Hf and Sm-Nd garnet geochronology: Chronometric closure and implications for dating petrological processes. Earth Planet. Sci. Lett. 381, 222–233.
Spear, F.S., 2010. Monazite-allanite phase relations in metapelites. Chem. Geol. 279, 55–62.
Spear, F.S., Pyle, J.M., 2002. Phosphates in metamorphic rocks. Rev. Mineralogy 48, 293–335.
Spear, F.S., Pyle, J.M., Cherniak, D., 2009. Limitations of chemical dating of monazite. Chem. Geol. 266, 218–230.
Steenken, A., Siegesmund, S., Heinrichs, T., 2000. The emplacement of the Rieserferner Pluton (Eastern Alps, Tyrol): constraints from field observations, magnetic fabrics and microstructures. J. Struct. Geol. 22, 1855–1873.
Steffen, K.J., Selverstone, J., 2006. Retrieval of *P-T* information from shear zones: thermobarometric consequences of changes in plagioclase deformation mechanisms. Contrib. Mineral. Petrol. 151, 600–614.
Steiger, R.H., Jäger, E., 1977. Subcommission on Geochronology: Convention on the use of decay constants in geo- and cosmochronology. Earth Planet. Sci. Lett. 36, 359–362.
Stipp, M., Stünitz, H., Heilbronner, R., Schmid, S.M., 2002. The eastern Tonale fault: A "natural laboratory" for crystal plastic deformation of quartz over a temperature range from 250 to 700°C. J. Struct. Geol. 24, 1861–1884.
Stipp, M., Fügenschuh, B., Gromet, L.P., Stünitz, H., Schmid, S.M., 2004. Contemporaneous plutonism and strike-slip faulting: A case study from the Tonale fault zone north of the Adamello pluton (Italian Alps). Tectonics 23, TC3004.
Streepey, M.M., Hall, C.M., van der Pluijm, B.A., 2002. The $^{40}Ar/^{39}Ar$ laser analysis of K-feldspar: constraints on the uplift history of the Grenville Province in Ontario and New York. J. Geophys. Res. 107, 2296.
Stünitz, H., 1998. Syndeformational recrystallization – dynamic or compositionally induced? Contrib. Mineral. Petrol. 131, 219–236.
Süssenberger, A., Brito Neves, B.B., Wemmer, K., 2014. Dating low-grade metamorphism and deformation of the Espinhaço Supergroup in the Chapada Diamantina (Bahia, NE Brazil): a K/Ar fine-fraction study. Braz. J. Geol. 44, 207–220.
Süssenberger, A., Schmidt, S.T., Wemmer, K., Baumgartner, L.P., Grobéty, B., 2017. Timing and thermal evolution of fold-and-thrust belt formation in the Ultima Esperanza District, 51°S Chile: Constraints from K-Ar dating and illite characterization. Geol. Soc. Am. Bull. https://doi.org/10.1130/B31766.1.
Suzuki, K., Kato, T., 2008. CHIME dating of monazite, xenotime, zircon and polycrase: protocol, pitfalls and chemical criterion of possible discordant age data. Gondwana Res. 14, 569–586.
Suzuki, K., Adachi, M., Tanaka, T., 1991. Middle Precambrian provenance of Jurassic sandstone in the Mino Terrane, central Japan: Th-U-total Pb evidence from an electron microprobe monazite study. Sediment. Geol. 75, 141–147.
Tagami, T., 2012. Thermochronological investigation of fault zones. Tectonophysics 538-540, 67–85.
Tchato, D.T., Schulz, B., Nzenti, J.-P., 2009. Electron microprobe dating and thermobarometry of Neoproterozoic metamorphic events in the Kekem area, Central African Fold Belt of Cameroon. N. Jb. Miner. Abh. 186, 95–109.
Teyssier, C., Tikoff, B., Markley, M., 1995. Oblique plate motion and continental tectonics. Geology 23, 447–450.
Tikoff, B., Teyssier, C., 1994. Strain modeling of displacement-field partitioning in transpressional orogens. J. Struct. Geol. 16, 1575–1588.
Torgersen, E., Viola, G., Zwingmann, H., Harris, C., 2014. Structural and temporal evolution of a reactivated brittle-ductile fault – Part II: Timing of fault initiation and reactivation by K-Ar dating of synkinematic illite/muscovite. Earth Planet. Sci. Lett. 407, 221–233.
van der Pluijm, B., Hall, C.M., 2015. Fault zone (Thermochronology). In: Rink, W.J., Thompson, J.W. (Eds.), Encyclopedia of Scientific Dating Methods. Springer, Dordrecht. https://doi.org/10.1007/978-94-007-6304-3.
van der Pluijm, V.A., Mezger, K., Cosca, M.A., Essene, E.J., 1994. Determining the significance of high-grade shear zones by using temperature-time paths, with examples from the Grenville orogen. Geology 22, 743–746.
van der Pluijm, B.A., Hall, C.M., Vrolijk, P.J., Pevear, D.R., Covey, M.C., 2001. The dating of shallow faults in the Earth's crust. Nature 412, 172–175.
van der Pluijm, B.A., Vrolijk, P.J., Pevear, D.R., Hall, C.M., Solum, J., 2006. Fault dating in the Canadian Rocky Mountains: Evidence for late Cretaceous and early Eocene orogenic pulses. Geology 34, 837–840.
Vauchez, A., Tommasi, A., Mainprice, D., 2012. Fault (shear zones) in the Earth's mantle. Tectonophysics 558-559, 1–27.
Vermeesch, P., 2015. Isotope Geology. Part I: Geochronology. University College London, London. https://doi.org/10.17605/OSF.IO/SJ4FT.
Verschure, R.H., Andriessen, P.A.M., Boelrijk, N.A.I.M., Hebeda, E.H., Maijer, C., Priem, H.N.A., Verdurmen, E.A.T., 1980. On the thermal stability of Rb-Sr and K-Ar biotite systems: Evidence from coexisting Sveconorwegian (ca 870 Ma) and Caledonian (ca 400 Ma) biotites in SW Norway. Contrib. Mineral. Petrol. 74, 245–252.
Viegas, L.G.F., Archanjo, C.J., Vauchez, A., 2013. Fabrics of migmatites and the relationships between partial melting and deformation in high-grade transpressional shear zones: The Espinho Branco anatexite (Borborema Province, NE Brazil). J. Struct. Geol. 48, 45–56.
Villa, I.M., 1998. Isotopic closure. Terra Nova 10, 42–47.
Villa, I.M., Bucher, S., Bousquet, R., Kleinhanns, I.C., Schmid, S.M., 2014. Dating polygenetic metamorphic assemblages along a transect across the Western Alps. J. Petrol. 55, 803–830.
Villa, I.M., De Bièvre, P., Holden, N.E., Renne, P.R., 2015. IUPAC-IUGS recommendation on the half life of ^{87}Rb. Geochim. Cosmochim. Acta 164, 382–385.
Viola, G., Scheiber, T., Fredin, O., Zwingmann, H., Margreth, A., Knies, J., 2016. Deconvoluting complex structural histories archived in brittle fault zones. Nat. Comms. 7, 13448.
Violay, M., Heap, M.J., Acosta, M., Madonna, C., 2017. Porosity evolution at the brittle-ductile transition in the continental crust: Implications for deep hydro-geothermal circulation. Sci. Rep. 7, 7705.
Vissers, R.L.M., van Hinsbergen, D.J.J., Wilkinson, C.M., Ganerød, M., 2016. Middle Jurassic shear zones at Cap de Creus (eastern Pyrenees, Spain): a record of pre-drift extension of the Piemonte-Ligurian Ocean? J. Geol. Soc. 174, 289–300.
Vitale, S., Mazzoli, S., 2008. Heterogeneous shear zone evolution: The role of shear strain hardening/softening. J. Struct. Geol. 30, 1383–1395.
Vitale, S., Mazzoli, S., 2010. Strain analysis of heterogeneous ductile shear zones based on the attitudes of planar markers. J. Struct. Geol. 32, 321–329.
Vry, J.K., Baker, J.A., 2006. LA-MC-ICPMS Pb-Pb dating of rutile from slowly cooled granulites: Confirmation of the high closure temperature for Pb diffusion in rutile. Geochim. Cosmochim. Acta 70, 1807–1820.
Wang, Y., Zwingmann, H., Zhou, L., Lo, C., Viola, G., Hao, J., 2016. Direct dating of folding events by $^{40}Ar/^{39}Ar$ analysis of synkinematic muscovite from flexural-slip planes. J. Struct. Geol. 83, 46–59.
Wawrzenitz, N., Krohe, A., Rhede, D., Romer, R.L., 2012. Dating rock deformation with monazite: The impact of dissolution precipitation creep. Lithos 134-135, 52–74.
Webb, L.E., Johnson, C.L., Minjin, C., 2010. Late Triassic sinistral shear in the East Gobi Fault Zone, Mongolia. Tectonophysics 495, 246–255.
Weinberg, R.F., Mark, G., 2008. Magma migration, folding, and disaggregation of migmatites in the Karakoram Shear Zone, Ladakh, NW India. Geol. Soc. Am. Bull. 120, 994–1009.
Wemmer, K., Ahrendt, H., 1997. Comparative K-Ar and Rb-Sr age determinations of retrograde processes on rocks from the KTB deep drilling project. Geol. Rundsch. 86, 272–285.
Wemmer, K., Steenken, A., Müller, S., López de Luchi, M.G., Siegesmund, S., 2011. The tectonic significance of K/Ar illite fine-fraction ages from the San Luis Formation (Eastern Sierras Pampeanas, Argentina). Int. J. Earth Sci. 100, 659–669.
Wheeler, J., 1987. The determination of true shear senses from the deflection of passive markers in shear zones. J. Geol. Soc. 144, 73–77.
White, A.P., Hodges, K.V., 2002. Multistage extensional evolution of the central East Greenland Caledonides. Tectonics 21, 1048.
Whitmeyer, S.J., 2008. Dating fault fabrics using modern techniques of $^{40}Ar/^{39}Ar$ thermochronology: evidence for Paleozoic deformation in the Eastern Sierras Pampeanas. Argentina. J Virtual Explorer. https://doi.org/10.3809/jvirtex.2008.00207.
Whitmeyer, S.J., Wintsch, R.P., 2005. Reaction localization and softening of texturally hardened mylonites in a reactivated fault zone, central Argentina. J. Metamorph. Geol. 23, 411–424.
Wiberley, C., 1999. Are feldspar-to-mica reactions necessarily reaction-softening processes in fault zones? J. Struct. Geol. 21, 1219–1227.
Williams, G., Dixon, J., 1982. Reaction and geometrical softening in granitoid mylonites. Texture Microstruct. 4, 223–239.
Williams, M.L., Jercinovic, M.J., 2012. Tectonic interpretation of metamorphic tectonites: integrating compositional mapping, microstructural analysis and *in situ* monazite dating. J. Metamorph. Geol. 30, 739–752.
Williams, M.L., Jercinovic, M.J., Goncalves, P., Mahan, K., 2006. Format and philosophy for collecting, compiling, and reporting microprobe monazite ages. Chem. Geol. 225, 1–15.
Williams, M.L., Jercinovic, M.J., Harlov, D.E., Budzyń, B., Hetherington, C.J., 2011. Resetting monazite ages during fluid-related alteration. Chem. Geol. 283, 218–225.
Wolff, R., Dunkl, I., Kiesselbach, G., Wemmer, K., Siegesmund, S., 2012. Thermochronological constraints on the multiphase exhumation history of the Ivrea-Verbano Zone of the Southern Alps. Tectonophysics 579, 104–117.
Xypolias, P., 2010. Vorticity analysis in shear zones: A review of methods and applications. J. Struct. Geol. 32, 2072–2092.
Yund, R.A., Tullis, J., 1991. Compositional changes of minerals associated with dynamic recrystallization. Contrib. Mineral. Petrol. 108, 346–355.
Zenk, M., Schulz, B., 2004. Zoned Ca-amphiboles and related P-T evolution in metabasites from the classical Barrovian metamorphic zones in Scotland. Mineral. Mag. 68, 769–786.
Zhu, Y., An, F., Tan, J., 2011. Geochemistry of hydrothermal gold deposits: A review. Geosci. Frontiers 2, 367–374.
Zwingmann, H., Mancktelow, N., 2004. Timing of Alpine fault gouges. Earth Planet. Sci. Lett. 223, 415–425.
Zwingmann, H., Yamada, K., Tagami, T., 2010. Timing of brittle deformation within the Nojima fault zone, Japan. Chem. Geol. 275, 176–185.